ARMY RESEARCH LABORATORY

Doppler Broadening of Acoustic Waves Scattered by Turbulence Flowing With a Horizontal Wind

George H. Goedecke, Roy C. Wood, and Harry J. Auvermann

ARL-TR-2131 July 2000

The findings in this report are not to be construed as an official Department of the Army position unless so designated by other authorized documents.

Citation of manufacturer's or trade names does not constitute an official endorsement or approval of the use thereof.

Destroy this report when it is no longer needed. Do not return it to the originator.

Army Research Laboratory

Adelphi, MD 20783-1197

ARL-TR-2131 July 2000

Doppler Broadening of Acoustic Waves Scattered by Turbulence Flowing With a Horizontal Wind

George H. Goedecke
New Mexico State University

Roy C. Wood
Armstrong Atlantic State University

Harry J. Auvermann
Computational and Information Sciences Directorate, ARL

Abstract

This report investigates the scattering of a monochromatic acoustic wave by an assumed unchanging atmospheric turbulence distribution that moves with a uniform constant horizontal wind. The source and detector are at rest at different positions in a ground-fixed frame. Theoretical expressions are derived for the scattered acoustic pressure at the detector. Because distances and scattering angles change with time as any turbulent fluctuation (turbule) flows through the scattering volume, the detector signal has a time-dependent Doppler frequency shift. A simple formula for the consequent frequency broadening is derived. A computer code is developed that calculates the scattered signal and its fast Fourier transform scattered by a single turbule, or by a collection of turbules of many different scale lengths. The code uses a new approximate but quite accurate time-shift algorithm that reduces the calculation time substantially. Several numerical results from this code are presented for a model scenario that is similar to a recent experimental scenario, with good agreement among spectral widths and shapes.

Contents

1 Introduction 1

2 Technical Discussion 3

2.1 Scattering by One Turbule 3

2.1.1 Geometry 3

2.1.2 Scattered Acoustic Pressure at Detector 4

2.1.3 Turbule Model 6

2.1.4 Spectral Broadening 7

2.2 Multiturbule Model 8

2.2.1 General Population 8

2.2.2 Time-Shift Algorithm 8

2.3 Results 10

3 Conclusions and Recommendations 24

References 27

Appendixes 29

A Theoretical Derivations 29

A-1 Geometry and Model 29

A-2 Acoustic Equations 30

A-3 Source Wave 30

A-4 Scattered Waves 34

A-5 Temperature Scattering 35

A-6 Velocity Scattering 38

B Computer Algorithm 41

B-1 **Detector and Source Locations and Wind** 41

B-2 **Spectral Analysis** 42

B-3 **Turbule Model Parameters** 44

C Quick Doppler Formula 47

D Computer Codes 49

Distribution 63

Report Documentation Page 67

Figures

1 Geometry in ground-fixed reference frame 3

2 Pressure signal amplitude scattered by temeprature and velocity fluctuations for one 1.5-m turbule 12

3 Frequency spectra due to temperature and velocity fluctuations for one 1.5-m turbule 13

4 Pressure signal amplitude scattered by temperature and velocity fluctuations for one 4.7-cm turbule 14

5 Signal frequency spectra scattered by temperature and velocity fluctuations for one 4.75-cm turbule 14

6 Pressure signal amplitude scattered by velocity fluctuations in one tube of 0.75-m turbules, equally spaced, with spins in same direction 15

7 Pressure signal amplitude scattered by velocity fluctuations for one tube of 0.75-m turbules, randomly spaced, with spins in same direction 15

8 Signal frequency spectrum scattered by velocity fluctuations for one tube of 0.75-m turbules, equally spaced, with spins in same direction 16

9 Signal frequency spectrum scattered by velocity fluctuations for one tube of 0.75-m turbules, randomly spaced, with spins in same direction 16

10 Signal frequency spectrum scattered by temperature fluctuations for one tube of 0.19-m turbules, equally spaced, using direct method 17

11 Signal frequency spectrum scattered by temperature fluctuations for one tube of 0.19-m turbules, randomly spaced, using direct method 17

12 Signal frequency spectrum scattered by temperature fluctuations for one tube of 0.19-m turbules, randomly spaced, using time-shift method 18

13 Signal frequency spectrum scattered by velocity fluctuations for one tube of 1.5-m turbules, randomly spaced, with spins in same direction and random spin directions 19

14 Signal frequency spectrum scattered by temperature fluctuations for one tube of 1.5-m turbules, randomly spaced, all with $\Gamma_T > 0$ and with $\pm\Gamma_T$ equally likely 20

15 Total frequency spectrum due to temperature and velocity fluctuations for two full tubes with sizes 1.5 m down to 4.7 cm . . . 21

16 Total frequency spectrum due to temperature and velocity fluctuations for two full tubes 22

17 Total frequency spectrum due to temperature and velocity fluctuations for all four full tubes 22

18 Comparison of experimental data with model 23

B-1 "Primed" coordinate system 41

B-2 Estimating minimum measurement time duration 43

B-3 Estimating maximum measurement time duration 44

D-1 Flow chart for main program 58

D-2 Flow chart for subroutine CHOICE 59

D-3 Flow chart for subroutine MULTI 60

D-4 Flow chart for subroutines ROTATE, DIRECT, and TAU 61

D-5 Flow chart for subroutines ONETRB, OUTPUT, and DOT 62

Tables

D-1 Intermediate save operations 62

1. Introduction

This report investigates acoustic scattering by atmospheric turbulence that is totally frozen (stationary) in a frame comoving with a uniform constant horizontal wind. The ambient temperature is also assumed constant and uniform. For convenience, the turbulence is modeled as an appropriate collection of self-similar eddies or "turbules," as described in past literature [1]. A turbule is a localized region of temperature and/or flow velocity fluctuations with respect to ambient values.

An acoustic detector and a monochromatic source are at rest in a ground-fixed frame at different positions. The detector and source are assumed to be in the far-field region of a turbule at any instant but in the near-field region of the complete stationary volume that the turbules traverse. This is almost always the case in experimental situations. The theory developed during this work first obtains a Born approximation expression for the time dependence of the acoustic pressure at the detector caused by scattering of the source pressure wave by one turbule. A computer algorithm developed during this work calculates this expression. This algorithm also calculates the fast Fourier transform (FFT) of this pressure wave and reveals that the wave's frequency spectrum is both shifted and broadened appreciably around the source frequency. The broadening occurs because the scattering angles and distances for any turbule are slowly varying functions of time for realistic wind speeds. A simple formula for the received frequency as a function of time is also derived by two different methods; it predicts the same broadening as the computer algorithm.

The conventional theory [2] does not allow for this kind of time dependence, because it assumes that the detector and source are in the far-field region of the whole scattering volume. Thus it predicts spectral broadening only if there are time-dependent fluctuations in the comoving frame. Establishing the amount of spectral broadening and shifting for turbulence completely frozen in the comoving frame but for realistic near-field detector and source locations thus became one of the most important objectives and results of this work. The experimentally observed spectral broadening used for comparison has a fairly narrow large peak around the source frequency that is very jagged but overall appears Gaussian, with wide noisy-looking wings at smaller amplitude. The theory developed in this report predicts that the large narrow peak is due to large turbules, but the wide wings are due to small ones, and also predicts that the jaggedness is due to randomness in turbule locations in the comoving frame. The computer algorithm based on the theory yields spectra that exhibit the same general features as some experimental data, including the spectral widths and jaggedness, for realistic populations of turbules of many length scales.

Also developed in this work is an efficient approximate method for adding contributions of many small turbules of each size that are approximately in-line with the wind. The method is demonstrated to be accurate, and it reduces computer running time significantly, enough so that three-dimensional modeling is indeed practical.

2. Technical Discussion

2.1 Scattering by One Turbule

2.1.1 Geometry

The scattering geometry is defined by figure 1. The letters S, D, and T stand for source, detector, and turbule, respectively. Coordinate z is vertical, $z = 0$ is the ground plane, and coordinates x and y are horizontal, ground-fixed. The uniform constant horizontal wind is $\mathbf{w}$, given by

$$\mathbf{w} = w(\mathbf{e}_x \cos\phi_w + \mathbf{e}_y \sin\phi_w) \,, \tag{1}$$

where $(\mathbf{e}_x, \mathbf{e}_y, \mathbf{e}_z)$ are the Cartesian unit basis vectors and ϕ_w is the azimuthal angle of the wind as shown. The source S and detector D are at locations given by position vectors $(\mathbf{R}^S, \mathbf{R}^D)$, respectively (fixed with respect to the ground-fixed reference frame) and the turbule center T has time-varying position vector $\mathbf{R}^T(t)$.

The location of the "center" of the turbule T is given by

$$\mathbf{R}^T(t) = \bar{\mathbf{b}} + \mathbf{w}t \,, \tag{2}$$

so $\bar{\mathbf{b}}$ is the location of the turbule at $t = 0$ in the ground-fixed frame.

The vectors $\mathbf{R}^{TS}$, $\mathbf{R}^{DT}$ are defined by

$$\mathbf{R}^{TS}(t) \equiv \mathbf{R}^T(t) - \mathbf{R}^S, \qquad \mathbf{R}^{DT}(t) = \mathbf{R}^D - \mathbf{R}^T(t) \,. \tag{3}$$

In the comoving (barred) frame, defined by

$$\bar{x} = x - w_x t, \quad \bar{y} = y - w_y t, \quad \bar{z} = z \,, \tag{4}$$

so that the origins coincide at $t = 0$, we have

$$\bar{\mathbf{R}}^T = \bar{\mathbf{b}} \,, \quad \bar{\mathbf{R}}^S(t) = \mathbf{R}^S - \mathbf{w}t \,, \qquad \bar{\mathbf{R}}^D(t) = \mathbf{R}^D - \mathbf{w}t \tag{5}$$

so that

$$\bar{\mathbf{R}}^{TS}(t) = \bar{\mathbf{R}}^T - \bar{\mathbf{R}}^S(t) = \bar{\mathbf{b}} - (\mathbf{R}^S - \mathbf{w}t) = \mathbf{R}^{TS}(t) \quad \text{and} \tag{6}$$

$$\bar{\mathbf{R}}^{DT}(t) = \bar{\mathbf{R}}^D(t) - \bar{\mathbf{R}}^T = \mathbf{R}^D - \mathbf{w}t - \bar{\mathbf{b}} = \mathbf{R}^{DT}(t) \,. \tag{7}$$

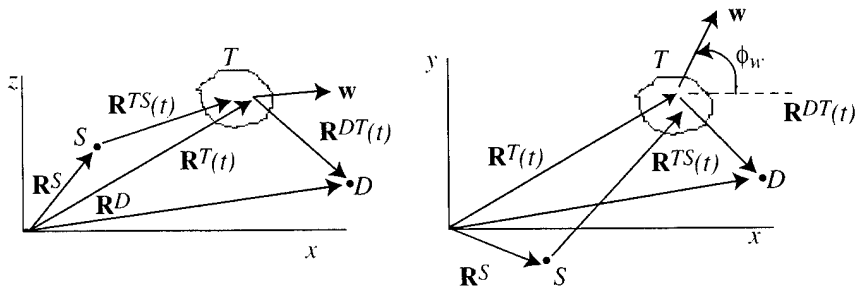

Figure 1. Geometry in ground-fixed reference frame.

2.1.2 Scattered Acoustic Pressure at Detector

We seek expressions for the acoustic pressure waves ($\bar{p}_{as}^{T}(t)$, $\bar{p}_{as}^{v}(t)$) scattered by the turbulent (temperature, velocity) fields of the turbule, as functions of time at the detector. These expressions are derived in detail in appendix A. Here, we quote the results valid to all orders of $\beta \equiv w/c$, where c is the ambient adiabatic sound speed, taken to be constant and uniform in the scattering volume in this work. The source is assumed to be monochromatic and isotropic in its rest (ground-fixed) frame. Reflections from the ground are ignored. From equation (A-71), we have for $\bar{p}_{as}^{T}(t)$ the form

$$\bar{p}_{as}^{T}(t) = A^{T}(t)\exp(-i\omega_s t) + \text{c.c.}\,. \tag{8}$$

where ω_s is the source angular frequency and $A^{T}(t)$ is a (slowly varying) complex-valued amplitude, given by equation (A-72):

$$A^{T}(t) = -\mathcal{P}_e\left(\frac{k_s^2 a'}{4\pi T_0 \gamma^2}\right)\left(\frac{(\bar{R}_0)^2}{(\bar{D}^s)^3 R^{DT}}\right)\left(\hat{\bar{\mathbf{R}}}_0 \cdot \hat{\mathbf{R}}^{DT}\right)\tilde{\bar{T}}(\mathbf{K})\exp[ik_s(\bar{R}_0 + R^{DT})]\,. \tag{9}$$

where a hat over a vector indicates that it is a unit vector. Here, $k_s = \omega_s/c$, $\mathcal{P}_e$ is the pressure of the source wave a distance a' from the source in a non-moving atmosphere, T_0 is the constant uniform ambient temperature, and $\tilde{\bar{T}}(\mathbf{K})$ is the spatial FFT of $\bar{T}(\bar{\mathbf{r}} - \bar{\mathbf{b}})$, the stationary temperature variation of the turbule in the comoving frame, given by

$$\tilde{\bar{T}}(\mathbf{K}) \equiv \int d^3\xi \bar{T}(\xi)\exp(-i\mathbf{K}\cdot\xi)\,. \tag{10}$$

Also, the various vectors and distances are defined by equations (A-65) to (A-70), as follows:

$$K_i = k_s\left\{\hat{R}_i^{DT} - \frac{\partial \bar{R}_0}{\partial \bar{b}_i}\right\}\,. \tag{11}$$

where

$$\frac{\partial \bar{R}_0}{\partial \bar{b}_i} = (\bar{D}^s)^{-1}(\delta_{ij} + \hat{R}_i^{DT}\beta_j)(\bar{R}_{0j})\,. \tag{12}$$

with

$$\bar{R}_{0j} = \bar{R}_j^s(t) - \beta_j \bar{R}_0 \tag{13}$$

$$\bar{R}_j^s = R_j^{TS}(t) - \beta_j R^{DT}(t) \tag{14}$$

$$\bar{D}^s = \left[(1-\beta^2)(\bar{R}^s)^2 - (\boldsymbol{\beta}\cdot\bar{\mathbf{R}}^s)^2\right]^{\frac{1}{2}} \tag{15}$$

$$\bar{R}_0 = (\bar{R}_{0j}\bar{R}_{0j})^{\frac{1}{2}} = \gamma^2\left\{\bar{D}^s - \boldsymbol{\beta}\cdot\bar{\mathbf{R}}^s\right\} \tag{16}$$

$$\beta_i \equiv w_i/c\,,\gamma \equiv (1-\beta^2)^{-\frac{1}{2}} \tag{17}$$

and with ($\mathbf{R}^{TS}(t)$, $\mathbf{R}^{DT}(t)$) given by equations (6) and (7). Note that all the quantities in equations (10) to (16) and thus $A^{T}(t)$ are functions of time that vary slowly compared to $\exp(-i\omega_s t)$.

These results are quite complicated, primarily because of retardation effects. Only when $\beta \to 0$ are they simple. Then we get

$$\overline{R}_{0j} \approx \overline{R}_{sj} \approx R_j^{TS}, \; \bar{D}^s \approx \bar{R}^s \approx R^{TS}. \tag{18}$$

$$K_i \approx k_s(\hat{R}_i^{DT} - \hat{R}_i^{TS}) \; . \quad \text{and} \tag{19}$$

$$A^T = -\mathcal{P}_e(k_s^2 a'/4\pi T_0)\left(\frac{\cos\theta}{R^{DT}R^{TS}}\right)\tilde{\bar{T}}(\mathbf{K})\exp[ik_s(R^{TS}+R^{DT})] \; . \tag{20}$$

where θ is the scattering angle, given here by

$$\cos\theta = \hat{\mathbf{R}}^{DT} \cdot \hat{\mathbf{R}}^{TS} \; . \tag{21}$$

These quantities are still weakly time dependent for $\beta <<< 1$. If we define

$$\begin{aligned} \hat{\mathbf{k}}_s = \; & \hat{\mathbf{R}}^{TS} \; , \quad A_{pw} = -\mathcal{P}_e a'(R^{TS})^{-1} \; \exp(ikR^{TS}) \; , \\ \hat{\mathbf{r}} \equiv \; & \hat{\mathbf{R}}^{DT} \; , \qquad r = R^{DT} \; , \end{aligned} \tag{22}$$

then the amplitude A^T of equation (20) has the form

$$A^T = A_{pw}\left(\frac{\exp(ik_s r)}{r}\right)\left(\frac{k_s^2\tilde{\bar{T}}(\mathbf{K})}{4\pi T_0}\right)\cos\theta \; , \tag{23}$$

with

$$\cos\theta = \hat{\mathbf{k}}_s \cdot \hat{\mathbf{r}} \quad , \quad \mathbf{K} = k_s(\hat{\mathbf{r}} - \hat{\mathbf{k}}_s) \; . \tag{24}$$

This is exactly the form of the Monin [3] result for temperature scattering from stationary turbulence, where A_{pw} is the amplitude of an incident plane wave traveling in direction $\hat{\mathbf{k}}_s$.

From equation (A-81), the contribution $p_{as}^v(t)$ scattered by the solenoidal turbulent velocity field of the turbule is

$$p_{as}^v(t) \; = A^v(t)\exp(-i\omega_s t) + \text{c.c.} \; , \tag{25}$$

where the complex amplitude $A^v(t)$ is defined by

$$A^v(t) \equiv \left(-\frac{k_s^2\mathcal{P}_e a'}{2\pi c\gamma^2}\right)\left\{\frac{\bar{R}_0^3(\hat{\bar{\mathbf{R}}}_0 \cdot \hat{\mathbf{R}}^{DT})(\hat{\mathbf{R}}^{DT} \cdot \tilde{\bar{\mathbf{v}}}\,(\mathbf{K}))}{(\bar{D}^s)^4 \; R^{DT}}\right\}\exp[ik_s(\bar{R}_0 + R^{DT})] \; , \tag{26}$$

with $\tilde{\bar{\mathbf{v}}}\,(\mathbf{K})$ the spatial FFT of the turbule velocity field $\bar{\mathbf{v}}(\bar{\mathbf{r}} - \bar{\mathbf{b}})$, stationary in the comoving (barred) frame, given by

$$\tilde{\bar{\mathbf{v}}}\,(\mathbf{K}) \equiv \int d^3\xi \exp(-i\mathbf{K}\cdot\boldsymbol{\xi})\bar{\mathbf{v}}(\boldsymbol{\xi}) \; . \tag{27}$$

For $\beta \to 0$, $A^v(t)$ also reduces to the Monin result for scattering by turbulent velocity fluctuations.

Equations (9) and (26), with the accompanying equations (10) to (17) and (27), are used in the computer algorithm described in appendix B. To obtain $\tilde{\bar{T}}(\mathbf{K})$ and $\tilde{\bar{\mathbf{v}}}\,(K)$ specifically, we must use a specific turbule model described in the following section.

2.1.3 Turbule Model

For convenience, we use Gaussian envelopes and spherical symmetry, as in a past paper [1]. A temperature turbule of scale length or "size" a, fixed in the comoving (barred) frame, is written

$$\bar{T}(\bar{\mathbf{r}} - \bar{\mathbf{b}}) = \Delta T_a \exp\left[-\frac{(\bar{\mathbf{r}} - \bar{\mathbf{b}})^2}{a^2}\right] . \tag{28}$$

and a velocity turbule of size a is written

$$\bar{\mathbf{v}}(\bar{\mathbf{r}} - \bar{\mathbf{b}}) = [\mathbf{\Omega}_a \times (\bar{\mathbf{r}} - \bar{\mathbf{b}})] \exp\left[-\frac{(\bar{\mathbf{r}} - \bar{\mathbf{b}})^2}{a^2}\right] . \tag{29}$$

Note that $\mathbf{\Omega}_a$ is an angular velocity, and $\bar{\mathbf{v}}$ is solenoidal.

The amplitudes (ΔT_a, $\Omega_a = |\mathbf{\Omega}_a|$) are scaled with a, as in a previous paper [1]. Specifically, we designate a_1 as the size of the largest turbule to be used, the outer scale length for this problem, and choose values for

$$\frac{\Delta T_1}{T_0} \equiv \Gamma_T \, , \frac{\Omega_1 a_1}{c} \equiv \Gamma_v \, . \tag{30}$$

Typical values are $\Gamma_T \approx \Gamma_v \approx 0.01$. Here, $\Omega_1 \equiv \Omega_{a_1}$, $\Delta T_1 \equiv \Delta T_{a_1}$. (We must also choose the direction $\hat{\mathbf{\Omega}}_a$.) Then, from the previous paper [1] and also in accordance with conventional models [2], we choose for any size a

$$\Delta T_a = (a/a_1)^{1/3} \Delta T_1 \, , \quad \Omega_a a = (a/a_1)^{1/3} \Omega_1 a_1 \, , \tag{31}$$

or

$$\Omega_a = (a_1/a)^{2/3} \Omega_1 \, . \tag{32}$$

From the definitions of equations (10) and (27) and from equations (28) and (29), we get the same expressions as in appendix A,

$$\tilde{\bar{T}}(\mathbf{K}) \;=\; \pi^{3/2} \, a^3 \, \Delta T_a \exp\left[\frac{-K^2 a^2}{4}\right] . \tag{33}$$

$$\tilde{\bar{\mathbf{v}}}\,(\mathbf{K}) \;=\; \frac{-i}{2} \pi^{3/2} a^5 \mathbf{\Omega}_a \times \mathbf{K} \exp\left[\frac{-K^2 a^2}{4}\right] . \tag{34}$$

Note that there is no velocity scattering if $\Omega_a \parallel \mathbf{K}$.

Consider the lowest-order approximation for the scattering vector $\mathbf{K}$, i.e., just like equation (19):

$$\mathbf{K}(t) \approx k_s(\hat{\mathbf{R}}^{DT}(t) - \hat{\mathbf{R}}^{TS}(t)) \, . \tag{35}$$

This is a good approximation if $\beta \ll 1$. Then

$$K^2 = 2k_s^2(1 - \cos\theta(t)) = 4k_s^2 \sin^2\left(\frac{\theta(t)}{2}\right) , \tag{36}$$

with the scattering angle $\theta(t)$ defined by equation (21). Therefore, if $k_s a \gg 1$, then $\tilde{\bar{T}}(\mathbf{K})$ and $\tilde{\bar{\mathbf{v}}}\,(\mathbf{K})$ are extremely small unless θ is near 0°, so the scattering is negligible at large angles. But for $k_s a \ll 1$, the Gaussian envelope in equations (33) and (34) is essentially unity for all scattering angles, so backward scattering is comparable to near forward scattering in magnitude.

2.1.4 Spectral Broadening

We note that both $A^T(t)$ and $A^v(t)$ contain the factor

$$\exp\{-i\omega_s[t - (\bar{R}_0(t) + R^{DT}(t))/c]\} \equiv \exp(-i\Phi(t)) \,. \tag{37}$$

where the equality defines the phase Φ. Consider any time $t = t_0$. Then write for t near t_0

$$\Phi(t) \approx \Phi(t_0) + (\dot{\Phi}(t_0))(t - t_0) + \text{ neglect} \,. \tag{38}$$

where we can neglect terms of higher order in $(t - t_0)$ if $\bar{R}_0(t)$ and $R^{DT}(t)$ are "slowly varying," which is the case for $\beta \ll 1$. Thus $\dot{\Phi}(t_0)$ is the effective angular frequency $\omega(t_0)$ at time t_0. Since t_0 is any time, we have

$$\omega(t) = \omega_s[1 - \frac{1}{c}(\dot{\bar{R}}_0(t) + \dot{R}^{DT}(t_0))] \,. \tag{39}$$

When equations (12), (3), and (13) to (17) are used, obtaining an expression for $\omega(t)$ valid to first order in β is very simple. Since c^{-1} times the time derivative of any position vector or distance is proportional to β, then for equations (13) to (17), we may put, to order β,

$$\dot{\bar{R}}_0(t) \approx \dot{R}^{TS}(t) = d_t(\mathbf{R}^{TS} \cdot \mathbf{R}^{TS})^{1/2} = \hat{\mathbf{R}}^{TS} \cdot \dot{\mathbf{R}}^{TS} = \mathbf{w} \cdot \hat{\mathbf{R}}^{TS} \tag{40}$$

$$\dot{R}^{DT}(t) = d_t(\mathbf{R}^{DT} \cdot \mathbf{R}^{DT})^{1/2} = \hat{\mathbf{R}}^{DT} \cdot \dot{\mathbf{R}}^{DT} = -\mathbf{w} \cdot \hat{\mathbf{R}}^{DT} \,. \tag{41}$$

Therefore, to order β,

$$\omega(t) \approx \omega_s[1 + \boldsymbol{\beta} \cdot (\hat{\mathbf{R}}^{DT}(t) - \hat{\mathbf{R}}^{TS}(t))] \,. \tag{42}$$

Note that this can be written in terms of the approximate scattering vector $\mathbf{K}(t)$ of equation (35) as

$$\omega(t) = \omega_s + \mathbf{w} \cdot \mathbf{K}(t) \,. \tag{43}$$

This relation is actually correct for the exact $\mathbf{K}(t)$ given by equation (11).

From equations (32) or (33), (36), and (33) and (34), and from figures 1(a) and 1(b), it is evident that small turbules may produce much wider spectral broadening than large ones. This is because the Gaussian envelope cuts off the scattering from large turbules when $|\mathbf{w} \cdot \mathbf{K}|$ is "large," but does not do so for small turbules. Thus from small turbules, we can get appreciable backscattering, so the relative frequency shift $\mathbf{w} \cdot \mathbf{K}\omega_s$ may vary from zero to $\pm 2\beta$, while for large turbules, $|\mathbf{w} \cdot \mathbf{K}|\omega_s \ll 2\beta$ for any scattering angles that produce appreciable scattering.

It should be emphasized that this general behavior is not peculiar to a turbule model, or to Gaussian model turbules, but is common for any model of turbulence that contains both large and small length scales and is frozen in a comoving frame, provided only that the source and detector are in the near-field region of the complete scattering volume V_s. This applies to the scenarios of interest in this work. If (and only if) the source and detector are both in the far-field region of V_s at all times, then the conventional result ensues that moving frozen turbulence may produce only a frequency shift but no broadening [2].

In appendix C, a different simple derivation of equation (42) is provided.

2.2 Multiturbule Model

This section contains a summary description of the scheme used later in the report for populating the scattering volume with turbules. Rather than having a continuous distribution of sizes for the turbule size parameter a, a discrete set of sizes a_n will be selected. For each size class index n, a cubical cell containing one turbule is defined whose linear dimension d_n is an appropriate multiple of a_n. Suppose that the time interval for which data are desired is T and that the average wind velocity is w. Then an approximate scattering volume length L is equal to wT. A tube is defined to be a region of space consisting of a sufficient number of cells M_n aligned along the wind direction so that the total length of the tube is L or greater. The several tubes for each size class n are stacked laterally and vertically to overspread the scattering volume. For this discussion, consider that $a_{n+1}/a_n = 1/2$. Then $d_{n+1}/d_n = 1/2$ and $M_{n+1}/M_n = 2$. The number of tubes for class $n+1$ is four times the number for class n.

2.2.1 General Population

Our interest is in the scattered acoustic pressure produced by a multiturbule model that contains appropriate numbers of turbules of many sizes, from the largest (outer scale) a_1 to the smallest (inner scale) a_{N_s}, with N_s different scales included. As shown by Goedecke et al [1], if we define the packing fraction

$$\phi = n_a a^3 \,, \tag{44}$$

where n_a is the number density of turbules of size a, then ϕ must be independent of a so that the energy transfer rate per unit mass in a Kolmogorov cascade can be scale-independent as well. On average, one turbule of size a is somewhere in each cubical cell of size d_a, where

$$d_a = n_a^{-1/3} = a/\phi^{1/3} \,. \tag{45}$$

For a typical $\phi \approx 10^{-3}$, $d_a = 10a$.

If we had unlimited computer resources, we could populate a defined scattering volume V_s with turbules of different sizes (one "randomly" located in each cell for each size) and simply add up the $(A^T(t),\ A^v(t))$ from each. This is actually what we do for the larger turbules with $k_s a \gtrsim 1$. But if there are perhaps 100 turbules with a = 2 m in V_s, then for a = 0.02 m = 2 cm, according to equation (44), there will be $(100)(2/0.02)^3 = 10^8$ turbules, a truly formidable number.

2.2.2 Time-Shift Algorithm

Fortunately, there seems to be a good approximate way to handle the multitude of smaller turbules that reduces the calculation time significantly. Imagine two identical turbules, 1 and 2, more or less in-line along the wind direction, chosen to be the x-direction. That is, let the centers of their two

cells have coordinates $(\bar{b}_{cx}^{(1)}, \bar{b}_{cy}^{(1)}, \bar{b}_{cz}^{(1)})$ and $(\bar{b}_{cx}^{(2)}, \bar{b}_{cy}^{(1)}, \bar{b}_{cz}^{(1)})$; i.e., their cells are in-line with the wind.

Now, consider equation (9) for $A_{(1)}^T(t)$, from turbule 1, and assume that the source and detector are always in the radiation zone of a comoving cell of side $d = a/\phi^{1/3}$ in which the turbule is located. This implies $R_{(1)}^{DT}(t)$ and $R_{(1)}^{TS}(t) \gg (d.\,\lambda.\,d^2/\lambda)$, whichever is greater, at all (or most) times. For such cases, vectors such as $(\mathbf{R}^{TS(1)}, \dots)$ can be replaced by $(\mathbf{R}_c^{TS(1)}, \dots)$, the vectors to the center of the cell, except in the factor $\exp[ik_s(\bar{R}_0^{(1)} + R^{DT(1)})]$. In this factor, we may write

$$\exp[ik_s(\bar{R}_0^{(1)} + R^{DT(1)})] \approx \exp[ik_s(\bar{R}_{0c}^{(1)} + R_c^{DT(1)})] \exp(-i\mathbf{K}_c^{(1)} \cdot \boldsymbol{\eta}_1)\,, \quad (46)$$

where $\boldsymbol{\eta}_1$ is the displacement of the center of turbule 1 from its cell center. So we get

$$A_{(1)}^T(t) = \mathcal{A}_{(1)}^T(t) \exp(-i\mathbf{K}_c^{(1)}(t) \cdot \boldsymbol{\eta}_1)\,, \quad (47)$$

where from equations (9) and (46), we have

$$\begin{aligned}\mathcal{A}_{(1)}^T(t) \;\equiv\; & -\mathcal{P}_e(k_s^{2\prime} a/4\pi T_{0_0}\gamma^2)[(\bar{R}_{0c}^{(1)})^2/(\bar{D}_c^{s(1)})^3 R_c^{DT(1)}] \\ & \times(\hat{\bar{\mathbf{R}}}_{0c}^{(1)} \cdot\; \hat{\mathbf{R}}_c^{DT(1)})\widetilde{\bar{T}}_0(\mathbf{K}_c^{(1)}) \exp[ik_s(R_{0c}^{(1)} + R_c^{DT(1)})]. \end{aligned} \quad (48)$$

That is, $\mathcal{A}_{(1)}^T(t)$ is the old $A_{(1)}^T(t)$ but calculated with vectors to the cell center times the phase factor $\exp[ik_s(R_{0c}^{(1)} + R_c^{DT(1)})]$.

Now, for turbule 2, clearly $(\mathcal{A}_{(2)}^T(t), \mathbf{K}_c^{(2)}(t))$ are simply time-shifted from $(\mathcal{A}_{(1)}^T(t), \mathbf{K}_c^{(1)}(t))$. That is, we have

$$\mathcal{A}_{(2)}^T(t) = \mathcal{A}_{(1)}^T(t + \tau_2)\,, \quad \mathbf{K}_c^{(2)}(t) = \mathbf{K}_c^{(1)}(t + \tau_2)\,, \quad (49)$$

where $\tau_2 \equiv w^{-1}(\bar{b}_{cx}^{(2)} - \bar{b}_{cx}^{(1)})$. For example, suppose turbule 2 is one cell ahead of turbule 1, so that $b_{cx}^{(2)} - b_{cx}^{(1)} = d$. Then $\tau_2 = d/w$, so $\mathcal{A}_{(2)}^T(t)$ is just like $\mathcal{A}_{(1)}^T(t)$, but occurs earlier.

Thus, the time-shift algorithm for a whole tube of M turbules of a given size, with cell centers equally spaced by d along the wind direction, is obviously

$$A_{\text{tube}}^T(t) = \sum_{\ell=1}^{M} \mathcal{A}_{(1)}^T(t + \tau_\ell) \exp[-i\mathbf{K}_c^{(1)}(t + \tau_\ell) \cdot \boldsymbol{\eta}_\ell]\,, \quad (50)$$

where

$$\tau_\ell = w^{-1}(\bar{b}_{cx}^{(\ell)} - \bar{b}_{cx}^{(1)}) = (\ell - 1)(d/w)\,, \quad (51)$$

and $\boldsymbol{\eta}_\ell$ is chosen "randomly" for each ℓ; i.e., $-d/4 \le (\eta_{\ell x}, \eta_{\ell y}, \eta_{\ell z}) \le d/4$, with uniform independent probabilities. So, for a given tube, we need to

compute the complicated functions $(\mathcal{A}^T_{(1)}(t),\ \mathbf{K}^{(1)}_c(t))$ only once; then, for each turbule ℓ in the tube, we choose an $\boldsymbol{\eta}_\ell$ and compute

$$A^T_{(\ell)}(t-\tau_\ell) = \mathcal{A}^T_{(1)}(t)\exp(-\mathbf{K}^{(1)}_c(t)\cdot\boldsymbol{\eta}_\ell)\,. \tag{52}$$

then simply time-shift this to get $A^T_{(\ell)}(t)$, and add that to the accumulated $A^T_{\text{tube}}(t)$.

By comparing with direct computation of the $A^T_{\text{tube}}(t)$ for the same tube and using the full equations (9) to (16) for each turbule with its center at the same set of random locations as $\boldsymbol{\eta}_\ell$ from above, we found that for $\nu_s = 500$ Hz, the time-shift algorithm is a good approximation for $d \lesssim 4$ m. However, the algorithm is not as good for $d \geq 8$ m, with R^{DT}_c and $R^{TS}_c \gtrsim 10$ m minimum but actually $\gtrsim 100$ m during the times of largest signal production. Since a direct computation involves ~100 operations per turbule and a time-shift of only ~5 operations, the computing time advantage of the time-shift algorithm is major.

These same considerations apply for the $A^v(t)$ of equation (26), except that we need a separate $\hat{\boldsymbol{\Omega}}$ for each turbule. For any turbule, we may write in general

$$A^v(t) = \hat{\boldsymbol{\Omega}}\cdot B^v(t)\,, \tag{53}$$

where from equations (26) and (34), we have

$$\mathbf{B}^v(t) = -\left(\frac{i\pi^{1/2}a^5\Omega\mathcal{P}_e a'}{4c\gamma^2}\right)\left(\frac{\bar{R}_0^3(\hat{\bar{\mathbf{R}}}_0\cdot\hat{\mathbf{R}}^{DT})}{(\bar{D}^s)^4 R^{DT}}\right)\exp(-K^2a^2/4)\exp[ik_s(\bar{R}_0+R^{DT})](\hat{\mathbf{R}}^{DT}\times\mathbf{K})\,. \tag{54}$$

The time-shift algorithm for a tube of M turbules along the wind is now

$$A^v_{\text{tube}}(t) = \sum_{\ell=1}^{m}\hat{\boldsymbol{\Omega}}_\ell\cdot\mathbf{B}^{v(1)}_{(c)}(t+\tau_\ell)\exp[-i\mathbf{K}^{(1)}_c(t+\tau_\ell)\cdot\boldsymbol{\eta}_\ell]\,. \tag{55}$$

where $(\mathbf{B}^{v(1)}_{(c)},\ \mathbf{K}^{(1)}_c(t))$ are calculated with vectors to the center of the cell containing and comoving with turbule 1. We calculate the same way as for $A^T_{\text{tube}}(t)$, except that we must choose an $\hat{\boldsymbol{\Omega}}_\ell$ as well as an $\boldsymbol{\eta}_\ell$ for each turbule.

2.3 Results

Many of the theoretical results are presented and discussed in the previous section and in appendixes A to C, so we limit this section primarily to presenting and discussing graphs that illustrate some of the most interesting predictions of the computer code (Slow Eddy) that was developed on the basis of the theoretical results. However, we will also show how the theory easily predicts the major features of these computational results.

For all the following results, the detector was placed at (−150, 0, 0) m and the source at (150, 0, 10) m, and the wind was chosen with components (3.1, 0, 0) m/s. Thus, the primed and unprimed ground-fixed frames described in section 2.1.1 and discussed in appendix B were the same, and the wind velocity was blowing from the detector toward the source, in the $(+x)$ direction. The total time T was 24 s, $0 \leq t < T$, tube length was $L = vT = 756.4$ m centered at the origin, the time steps Δt were 0.0403 s, and the total number of points used in the calculation was $N = 6048$. (The point $n = 6049 \leftrightarrow t = T$ is "equivalent" to $t = 0$ because of the inherent periodicity of the discrete FFT.) The adiabatic sound speed was taken to be $c = 340$ m/s, corresponding to an ambient temperature $T_0 \approx 15$ °C ≈ 288 K ≈ 60 °F. For multiturbule computations, each turbule angular velocity unit vector was generally chosen to have uniform random distribution in 4π solid angle, independently of other turbules. This orientation distribution produces a model of isotropic turbulence, as was discussed in another paper [1]. The ΔT_a in the scattering volume V_s were generally chosen to have the same sign (positive) because temperature turbules are air pockets warmer than ambient that have risen from the ground because of buoyancy forces, such as those over a paved runway that was used in the relevant experiment. Over a larger volume, the mean ΔT probably should be zero. In the following results, one calculation was made with each turbule ΔT either > 0 or < 0 with equal probability to contrast the results of the different conditions. Also, some calculations were made with the angular velocity vectors of the larger turbules all in the $+y$-direction, for the same reason.

The ratio of cell size to turbule size was chosen to be $d/a = 8$, yielding a packing fraction $\phi = 1.95 \times 10^{-3}$. The number of sizes in the cascade was chosen to be $N_s = 6$, and the (largest, smallest) turbule sizes (a_1, a_{N_s}) were chosen as (1.5 m, 0.046825 m), respectively. Thus the parameter N_d of equation (B-18) was equal to 2 (whereby $\mu = \ln 2$), such that each successively smaller size was half the previous size. The relative fluctuation strengths $(\Delta T_1/T_0 \equiv \Gamma_T, \Omega_1 a_1/c \equiv \Gamma_v)$ of equation (30) were chosen as $(\Gamma_T = 0.013, \Gamma_v = 0.027)$. From our previous paper [1] or equation (B-17) of this report, these values yield $C_v^2 = 0.088\ \mathrm{m}^{4/3}/\mathrm{s}^2, C_T^2 = 0.044\ \mathrm{K}^2/\mathrm{m}^{2/3}$. These values are in good agreement with those given by Brown and Clifford [4]. Also, this value of C_v^2 was inferred* from wind data that were measured, along with the time-dependent acoustic pressure received by many different detectors, during an experiment by Galindo and Havelock [5]. All the numerical values chosen in this report are supposed to provide a good approximation to those that existed in that experiment. (As mentioned earlier, a main objective of this work is to determine whether a realistic model of acoustic scattering by turbulence that is frozen in a frame and comoving with a wind can possibly simulate actual experimental results.)

Using these values of the input parameters and the method and computer code described in this subsection and in appendix B, we calculated total

*D. K. Wilson of ARL computed this value.

time-dependent complex acoustic pressure amplitudes $(A^T(t), A^v(t))$ scattered by individual turbules, tubes of turbules, and all tubes of turbules in several different scattering volumes and then Fourier transformed to get the spectra $(\tilde{A}^T(\omega), \tilde{A}^v(\omega))$. For convenience, each (A^T, A^v) of equations (9) and (26) was "normalized" by division by the factor $\mathcal{P}_r$ with $a' = 1$ m. Thus, $\mathcal{P}_r$ is now the pressure amplitude of the source wave at a distance $a' = 1$ m from the source in a still atmosphere. In what follows, the (A^T, A^v) are the normalized ones, which are dimensionless.

In figure 2, we plot the real and imaginary parts and the magnitudes of $(A^T(t), A^v(t))$, respectively, for a single turbule with $a = a_1 = 1.5$ m, with $\bar{b}_x = -L/2$, $\bar{b}_y = 0$, $\bar{b}_z = 20$ m. Here, $\bar{b}_z = 20$ m corresponds to an above-ground base height $z_b = 14$ m, plus $d_1/2 = 6$ m, half the side of a cubical cell having $d_1 = 8a_1$. In figure 3, we plot the magnitudes of the FFTs $\tilde{A}^T(\omega)$ and $\tilde{A}^v(\omega)$. One can easily understand from equation (33) why the pulse in figure 2 has a fairly narrow width in time: The Gaussian envelope rapidly kills the signal as the scattering angle increases, since $k_s a_1 \approx 13.9$. The frequency width can be obtained easily from equation (42), $\omega(t) \approx \omega_s[1 + \beta \cdot (\hat{\mathbf{R}}^{DT}(t) - \hat{\mathbf{R}}^{TS}(t))]$. That is, calculate or obtain from figure

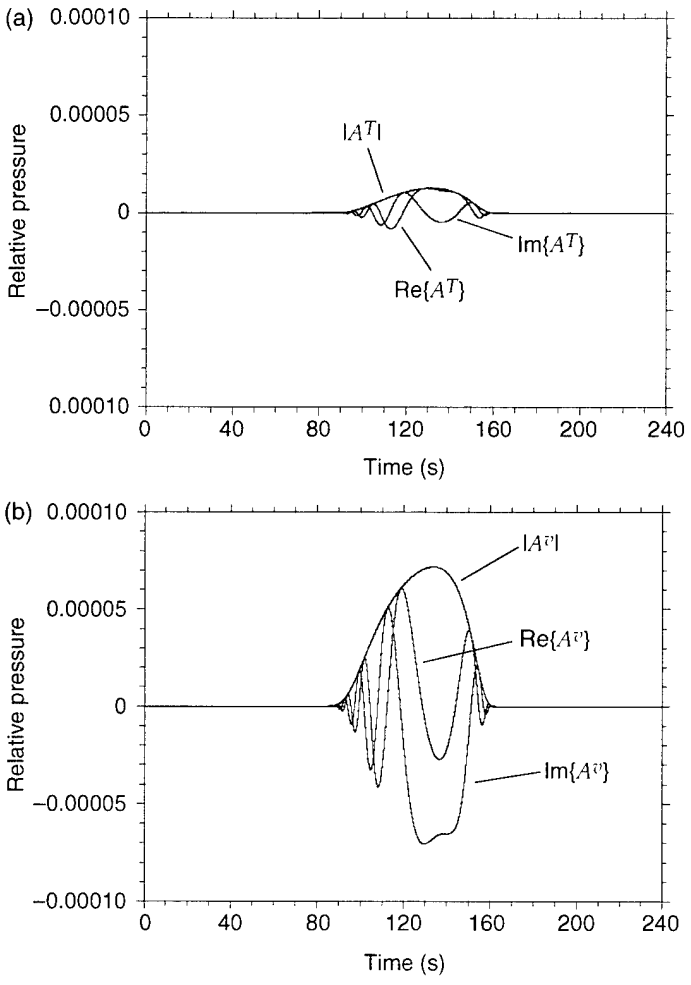

Figure 2. Pressure signal amplitude scattered by (a) temperature and (b) velocity fluctuations for one 1.5-m turbule.

2 the two times (t_1, t_2) at which the time-dependent magnitudes $\mid A(t) \mid$ are perhaps 5 percent oftheir maximum values and find $\hat{\mathbf{R}}^{DT}$ and $\hat{\mathbf{R}}^{TS}$ at these times. Then verify from figure 3 that $\mid \omega(t_1) - \omega(t_2) \mid$ is a good estimate of the (angular) frequency width of the $\tilde{A}(\omega)$. This calculation works because the complete frequency range $\nu_s(1 - 2\beta)$ to $\nu_s(1 + 2\beta)$ is "scanned" by any turbule, but only a small part of it is manifested in the scattered waves from large turbules.

In figures 4 and 5, we repeat the presentations of figures 2 and 3, respectively, but for a single small turbule of size $a_6 = 4.6875$ cm, with the same $(\bar{b}_x, \bar{b}_y, \bar{b}_z)$. For this size turbule, $(k_s a_6)^2 = 0.188$, so the Gaussian envelope of the $A(t)$ is almost unity for all scattering angles. Therefore, each $A(t)$ is nonzero over the total time duration, and the frequency width extends to almost the maximum possible, $\pm 2\beta\nu_s$, obtainable by backscattering from equation (42). Note also that each $\tilde{A}(\omega)$ goes to zero at frequencies $\nu_+ = 4.3$ Hz, $\nu_- = -4.2$ Hz. Again, this is easily understood from equations (9), (26), and (42): The time-dependent amplitude $A(t)$ is zero approximately when $\hat{\mathbf{R}}^{DT} \cdot \hat{\mathbf{R}}^{TS} = \cos\theta = 0$ (to lowest order in β). From figure 3, obtain the times t_3, t_4 at which this is true, and then use equation (42) to get $\omega(t_3)$ and $\omega(t_4)$; these agree quite well (within 5–10%) with the frequencies $\nu_\pm$. (The algebraic results are very sensitive to (t_3, t_4) values, and the computer algorithm contains higher order terms in β that slightly influence the results.) Also note the asymmetry of the $A(t)$ and $\tilde{A}(\omega)$; this is due to the source height being different from the detector height, in this geometry.

Figures 6 to 9 contrast the effects of randomness versus regularity in turbule center locations for many turbules. In figure 6, we present $|A^v(t)|$ for a tube of turbules with $a = 0.75$ m, with all angular velocities in the y-direction and each turbule center at the center of its comoving cell of side length $d_a = 8a = 6$ m. This tube forms a moving "diffraction grating." The tube centerline is $(\bar{b}_y = 0, \bar{b}_z = 20$ m), and there are $M_a = L/d_a = 126$ turbules contributing at any time. (In all calculations done for tubes, each cell in a

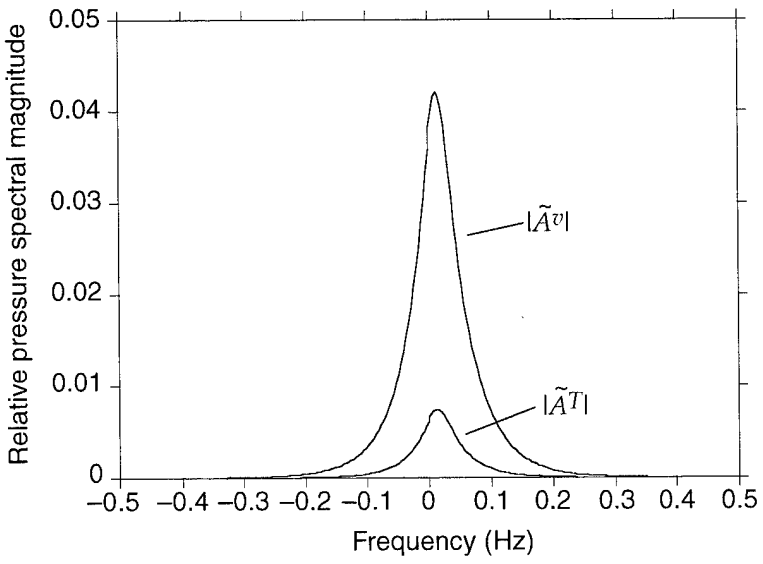

Figure 3. Frequency spectra due to temperature and velocity fluctuations for one 1.5-m turbule.

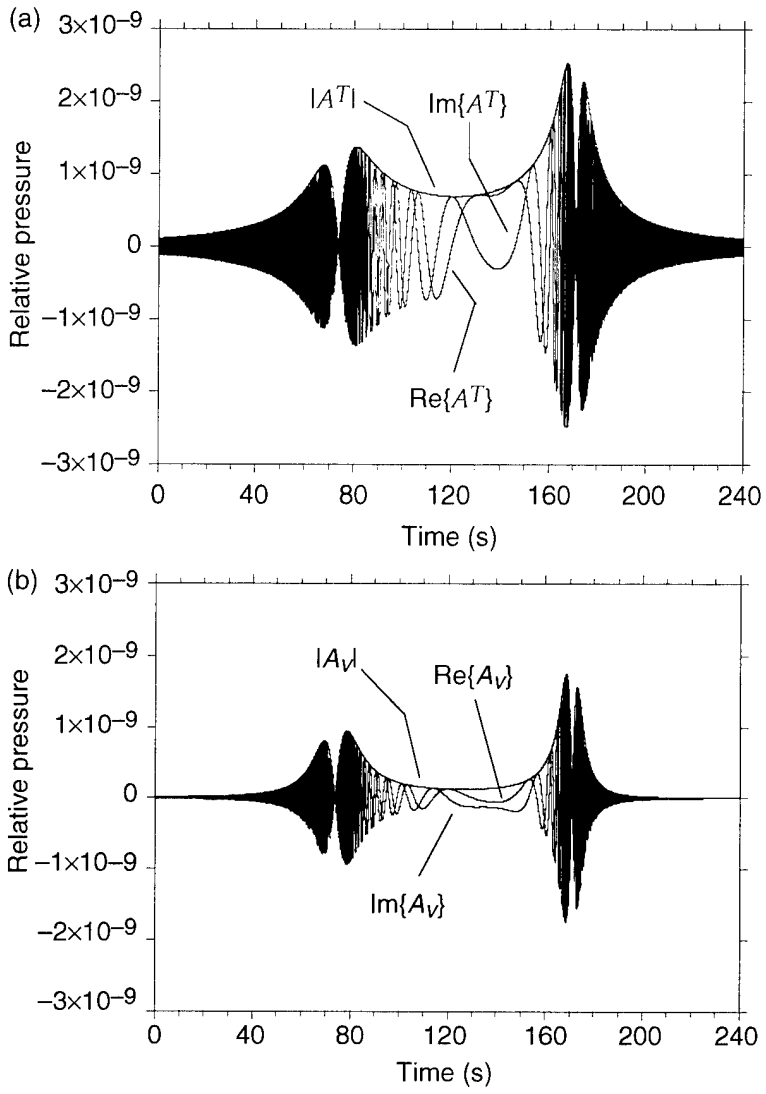

Figure 4. Pressure signal amplitude scattered by (a) temperature and (b) velocity fluctuations for one 4.7-cm turbule.

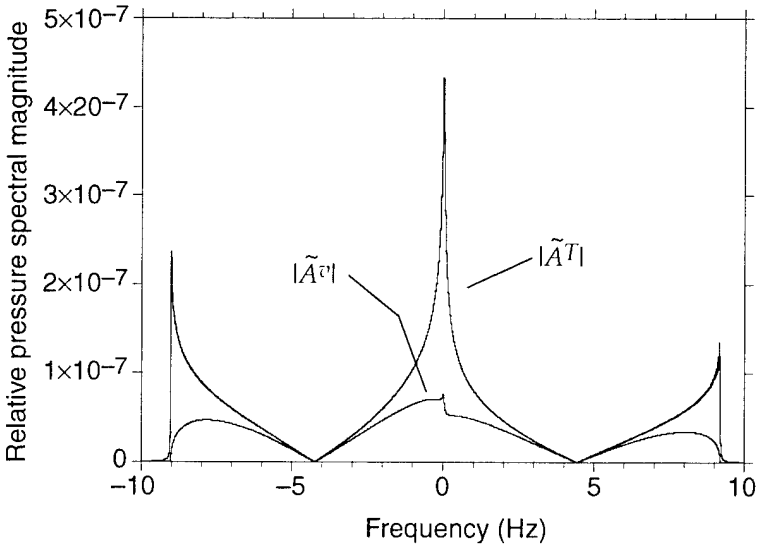

Figure 5. Signal frequency spectra scattered by temperature and velocity fluctuations for one 4.75-cm turbule.

fixed tube of total length L is kept filled; i.e., as a turbule is leaving at $L/2$, another is entering at $-L/2$. This ensures steady-state conditions.) The time dependence is extremely regular, as one would expect.

Figure 7 is for the same conditions as figure 6, except that each turbule center is randomly placed inside its comoving cell, with no correlations among placements of different turbules. The randomness consists of uniform uncorrelated probabilities of a turbule center's (x, y, z) locations being between $-d/4$ and $d/4$ from its comoving cell center. It is interesting (but totally expected) that this randomness produces extremely large relative fluctuations.

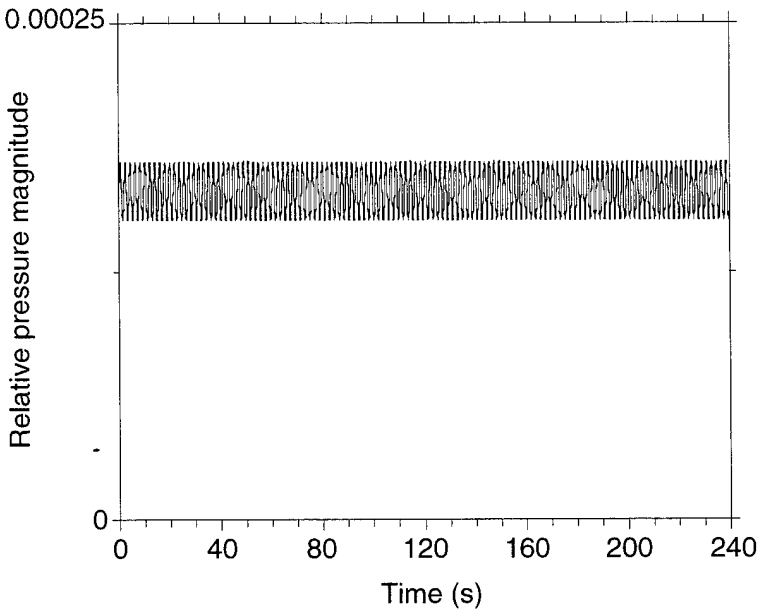

Figure 6. Pressure signal amplitude scattered by velocity fluctuations in one tube of 0.75-m turbules, equally spaced, with spins in same direction.

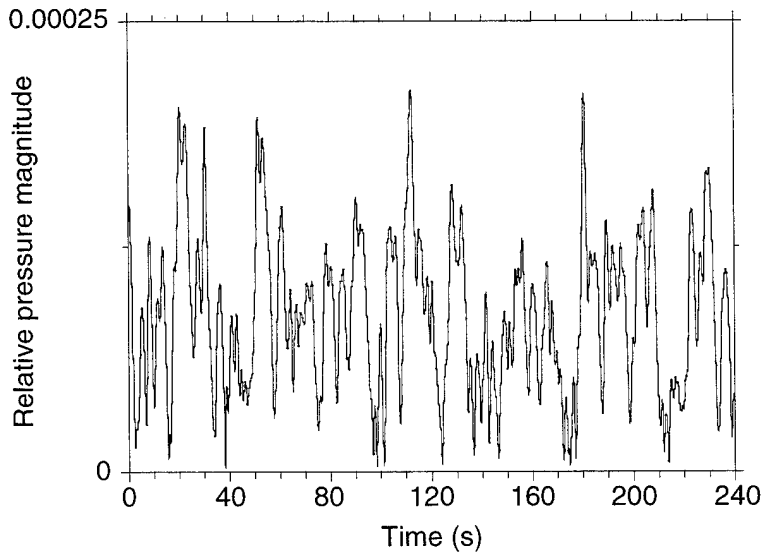

Figure 7. Pressure signal amplitude scattered by velocity fluctuations for one tube of 0.75-m turbules, randomly spaced, with spins in same direction.

In figures 8 and 9, we plot the magnitudes of the FFTs for the conditions of figures 6 and 7, respectively, on a semilog plot for good visibility. In figure 8, the principal maxima are striking; they are spaced just as they should be, i.e., at frequencies $\nu_q = qM_a/T \approx (q)(0.516)$ Hz, where q is an integer. There should be exactly zero contribution for other frequencies, for the discrete FFT. The principal maxima diminish rapidly as $|\nu|$ increases, probably because of the Gaussian envelope of a single turbule. (The picture is analogous to a multiple-slit interference pattern as modified by the single-slit diffraction pattern, in optics.) In figure 9, the randomness in turbule placement yields a jagged continuous spectrum. Both figures 8 and 9 display a remarkable straight-line behavior, which corresponds on these semilog plots to an exponential spectral envelope, $\exp(-|\nu|\tau_a)$, where τ_a is a constant with the dimension of time that most likely depends on the scale length a. We have not yet been able to predict this behavior theoretically.

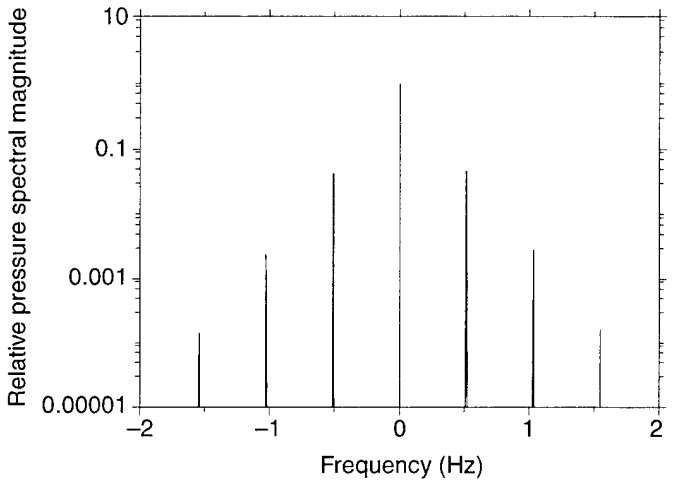

Figure 8. Signal frequency spectrum scattered by velocity fluctuations for one tube of 0.75-m turbules, equally spaced, with spins in same direction.

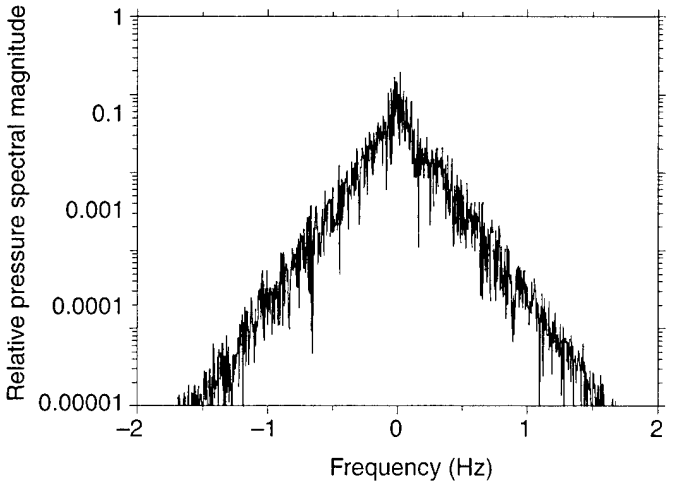

Figure 9. Signal frequency spectra scattered by velocity fluctuations for one tube of 0.75-m turbules, randomly spaced, with spins in same direction.

Figures 10 to 12 are intended to illustrate that the time-shift algorithm gives results essentially the same as direct calculation. These figures are $|\tilde{A}^T(\omega)|$ for a tube of $M_a = 504$ turbules with $a = 1.5/2^3 = 0.1875$ m, with the centerline as previously mentioned, with all $\Delta T_a > 0$. Figure 10 is for regular placement (for reference), with the use of "either" the direct or the time-shift calculation; i.e., the results are identical for regular placement of the turbule centers at their cell centers initially. Figure 11 is for random placements using the direct calculation. Figure 12 is for the "same" random placements but using the time-shift calculation, which is eight times faster than the direct method. Clearly the two methods produce substantially the same results, although there are small differences, as there should be, because the time-shift method is not exact.

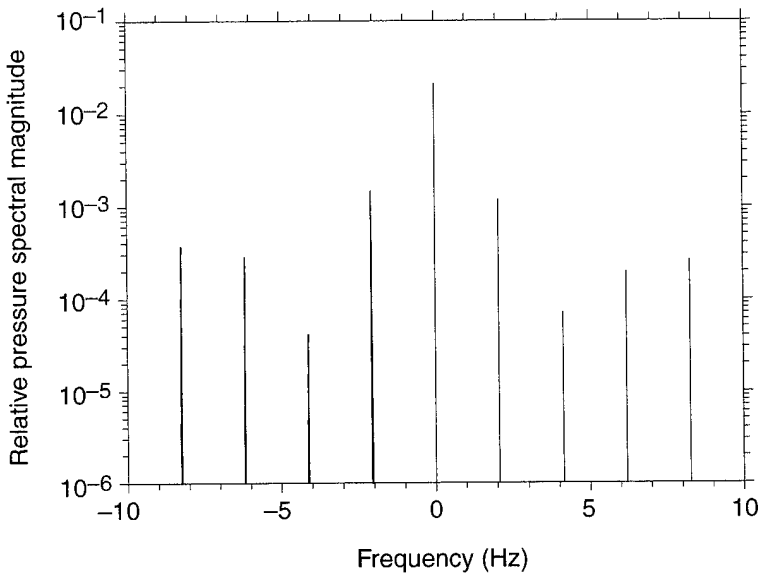

Figure 10. Signal frequency spectrum scattered by temperature fluctuations for one tube of 0.19-m turbules, equally spaced, using direct method.

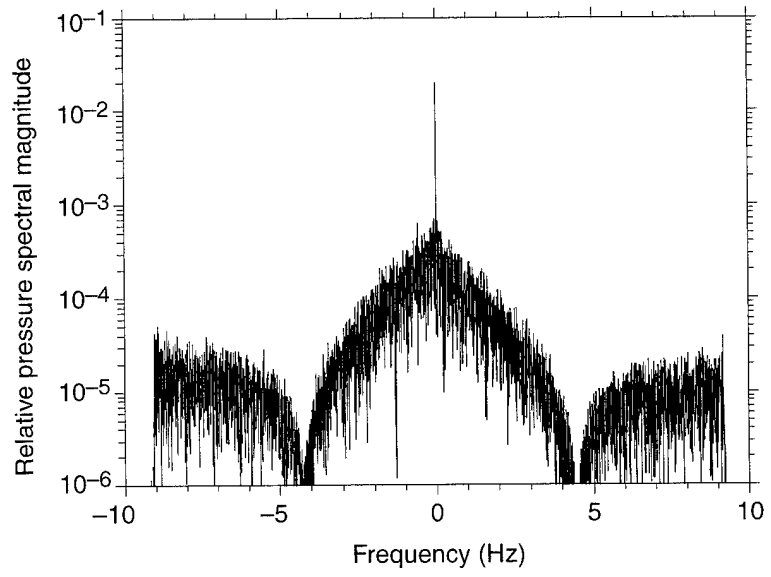

Figure 11. Signal frequency spectrum scattered by temperature fluctuations for one tube of 0.19-m turbules, randomly spaced, using direct method.

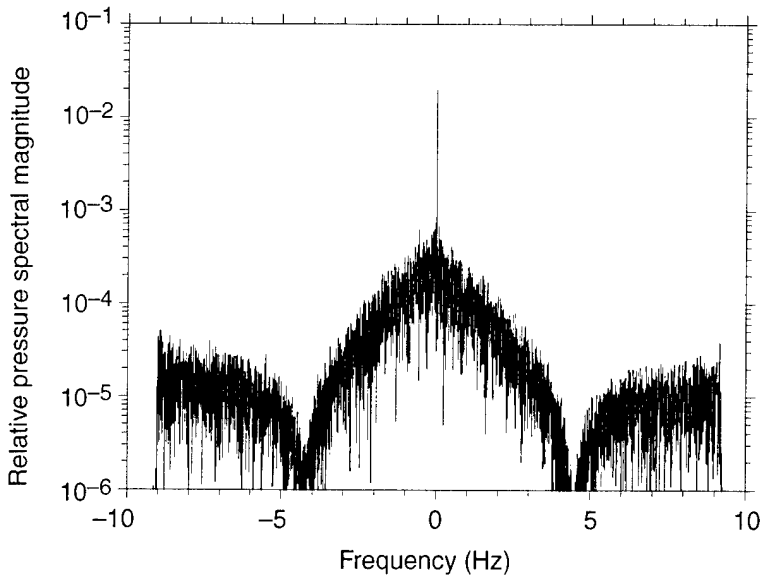

Figure 12. Signal frequency spectrum scattered by temperature fluctuations for one tube of 0.19-m turbules, randomly spaced, using time-shift method.

Figures 13 and 14 illustrate the effects of random versus nonrandom angular velocity directions $\hat{\Omega}$ and temperature amplitude signs $\Delta T/|\Delta T|$. They are for a tube of $M_a = 63$ turbules with $a = 1.5$ m, with the centerline at $b_y = 6$ m, $b_z = 20$ m. Figure 13 plots $|\tilde{A}^v(\omega)|$; figure 13(a) is for all the $\hat{\Omega}$ in the y-direction, while figure 13(b) is for the $\hat{\Omega}$ chosen isotropically at random. Figure 14 plots $|\tilde{A}^T(\omega)|$; figure 14(a) is for all $\Delta T > 0$, while figure 14(b) is for $\mathrm{sgn}(\Delta T) = \pm 1$ with equal probability (this would make T_0 equal to the mean temperature in V_s). In each case, the turbule center locations were randomized with the same set of random numbers, so differences in the comparable graphs must be caused by the different choices of $\hat{\Omega}$ or $\mathrm{sgn}(\Delta T)$. What is remarkable is that the differences are not large. This can be understood by noting that, for example, changing the sign of $\Delta T/|\Delta T|$ for a given turbule introduces a phase change of π in its scattered wave, which could have been done equally well by moving its center about a half wavelength. So, in general, randomization of $\hat{\Omega}$ and $\Delta T/|\Delta T|$ is nearly equivalent to nonrandomization with a little more "freedom of movement" of the turbule centers.

Figure 13. Signal frequency spectrum scattered by velocity fluctuations for one tube of 1.5-m turbules, randomly spaced, with (a) spins in same direction and (b) random spin directions.

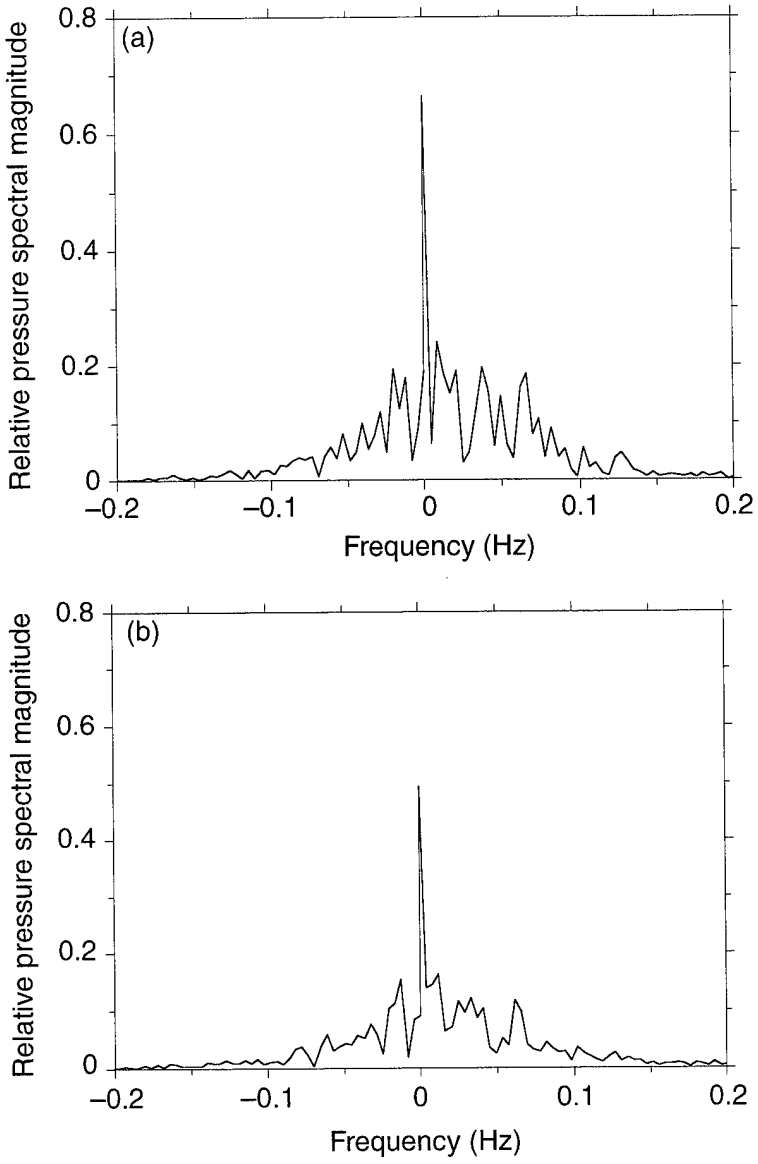

Figure 14. Signal frequency spectrum scattered by temperature fluctuations for one tube of 1.5-m turbules, randomly spaced, (a) all with $\Gamma_T > 0$ and (b) with $\pm\Gamma_T$ equally likely.

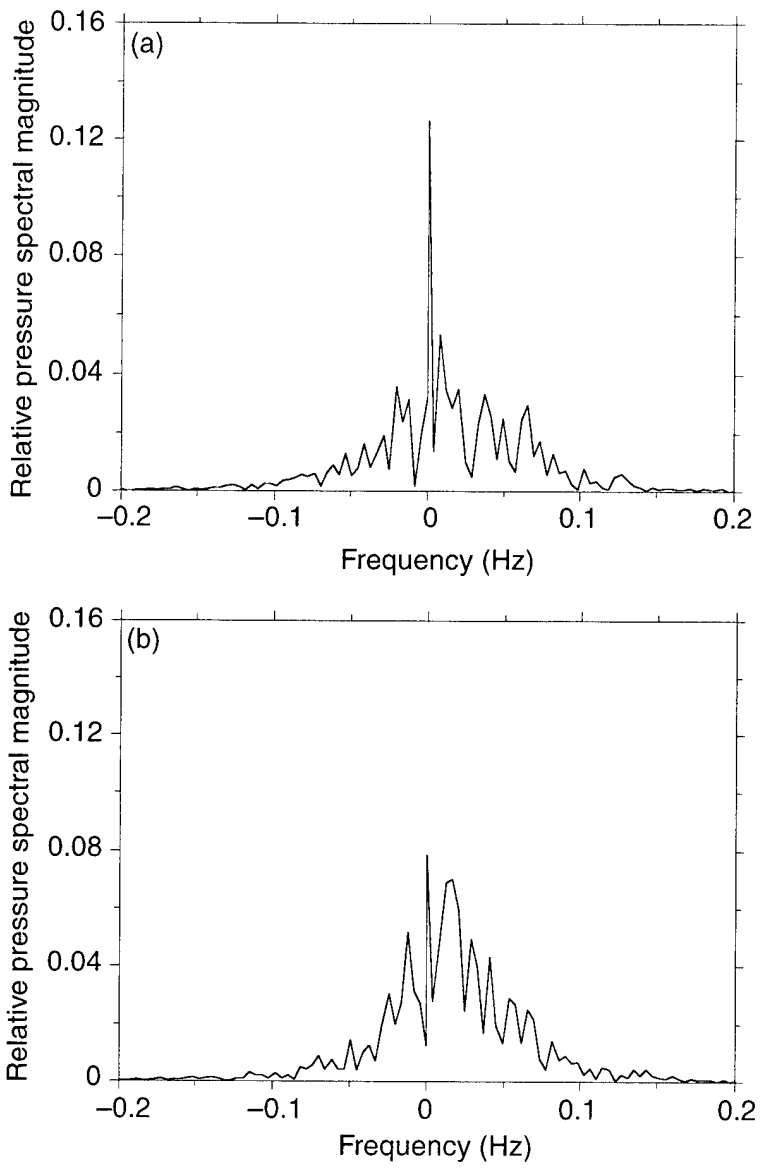

Figures 15 to 17 are sums over contributions of many turbules of all sizes used, i.e., a_α = (1.5, 0.75, 0.375, 0.1875, 0.09375, 0.046875) m for α = (1, ..., N_s = 6), respectively. The amplitudes $(\Omega_a, |\Delta T_a|)$ were scaled as discussed earlier, so these calculations are an attempt to numerically represent realistic, isotropic, homogeneous, fully developed turbulence by a turbule model, following the formulas by Goedecke and Auvermann [1]. This attempt is a compromise with the computing power of a PC with a Pentium II 233 MHz processor. We really should have included both larger and smaller turbules, plus many more different sizes in between. But what we did already required ~4.25 hr per large tube ($d_1 = 8a_1 = 12$ m), corresponding to 30 s per turbule, and this was only after we compromised further by making a reasonable approximation for the smallest size $a_6 = 0.046875$ m. We randomly put only "one" such turbule instead of eight in each cell of the next "larger" size, $d_5 = 8a_5 = 0.75$ m, and then we multiplied the result by eight. We checked this for a single tube of side length d_5 versus the "correct" method using turbules of scale a_6 only, and the results were quite close. Since so many such tubes are in one big tube ($(d_1/d_5)^2 = 256$), the total error induced by this economy should be quite small.

Figure 15 plots $|\tilde{A}^T(\omega) + \tilde{A}^v(\omega)|$ for two big tubes with centerlines $b_y = \pm 6$ m, $b_z = 20$ m. Figure 16 does the same for two big tubes above those of figure 15: i.e., $b_y = \pm 6$ m, $b_z = 32$ m. Figure 17 is the total frequency spectrum from these four tubes. Note that the contributions from the higher big tubes are significantly smaller, and that the general shapes of the plots are essentially unchanged, so these shapes are established already by just one or two tubes. The semilog plots clearly show the contributions of the small turbules all the way to $\pm 2\beta v_s = \pm 10$ Hz.

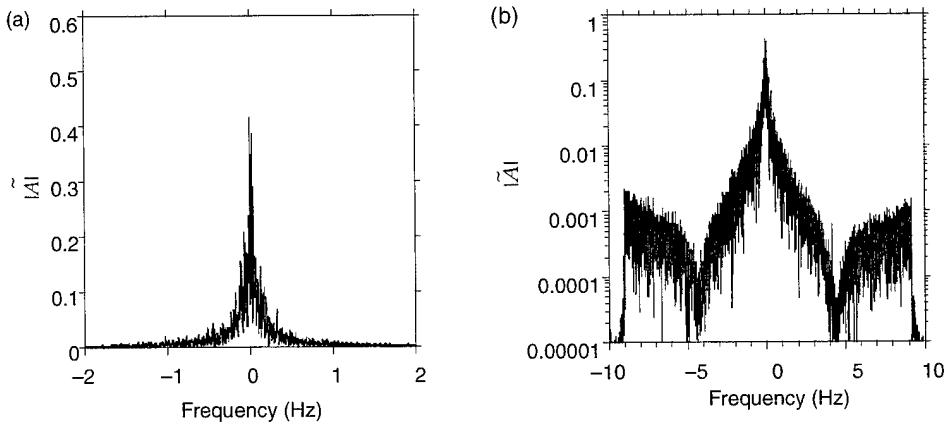

Figure 15. (a) Total frequency spectrum due to temperature and velocity fluctuations for two full tubes with sizes 1.5 m down to 4.7 cm. (b) Log plot of (a) from ± 10 Hz.

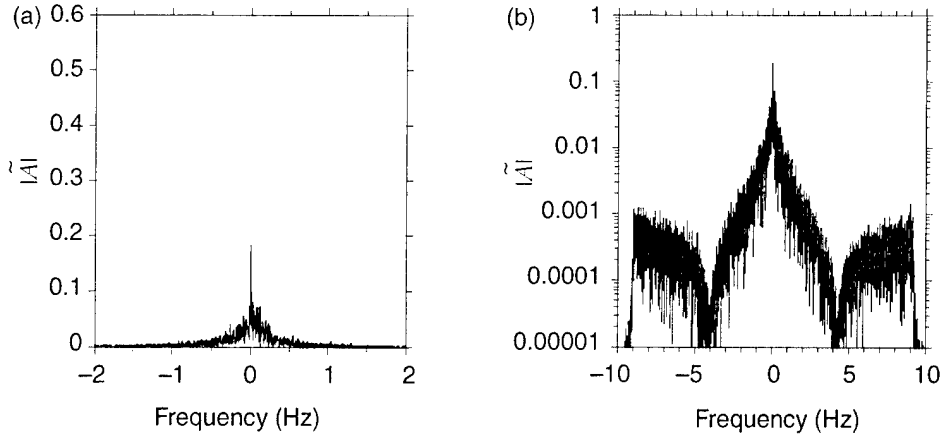

Figure 16. (a) Total frequency spectrum due to temperature and velocity fluctuations for two full tubes located above the two tubes in figure 14, with sizes 1.5 m down to 4.7 cm. (b) Log plot of (a) from ± 10 Hz.

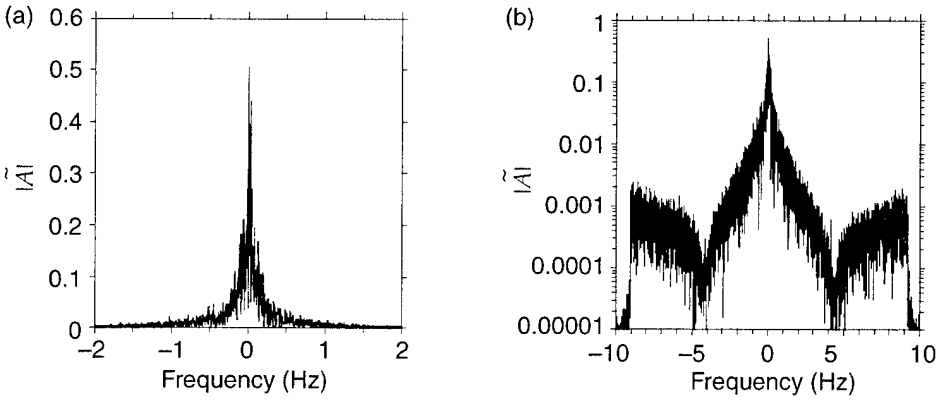

Figure 17. (a) Total frequency spectrum due to temperature and velocity fluctuations for all four full tubes from figure 14 and 15. (b) Log plot of (a) from ± 10 Hz.

Finally, figure 18 contrasts some experimental data with our model results. Figure 18(a) is from a presentation by Auvermann and Goedecke [6]; the jagged curve is the data. The central spike is about 101.56 Hz; this corresponds to $\nu = 0$ in the previous spectral plots and in figure 18(b). The ratio of the central spike height to the "mean" height at $\nu = 102 - 101.56 = 0.44$ Hz is about $6/0.23 = 26$. These data were for a source detector and wind velocity scenario very similar (but not identical) to what we modeled.

Figure 18(b) is an expansion of our figure 17(a) along the abscissa to match the total frequency width in figure 18(a). The model predictions are similar to the experimental results; e.g, the ratio of the central spike height (at $\nu = 0$) to the "mean" height at $\nu = 0.44$ Hz is $\approx 0.52/0.02 = 26$, in figure 18(b). But the jaggedness in the model results is not as great as in the experimental results. In later investigations, it has been found that the jaggedness, defined as the mean frequency spacing of adjacent peaks and valleys in the spectrum, is approximately equal to $3/T$, where T is the duration of the time signal. The model jaggedness agrees with the experimental jaggedness, if T is the same for both.

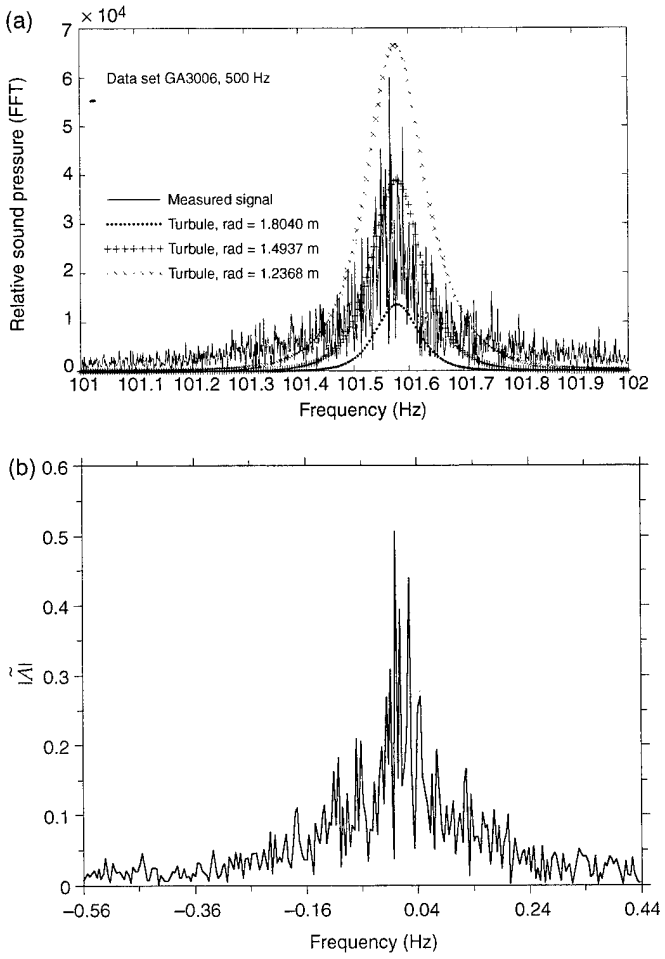

Figure 18. Comparison of experimental data with model: (a) Frequency spectrum from experiment and (b) frequency spectrum from figure 17(a).

3. Conclusions and Recommendations

The theory developed in this work allows understanding of the spectral broadening and shifting in an acoustic wave scattered from moving turbulence on the basis of two simple general physical principles. The first principle is that, even if the turbulence is frozen in a frame comoving with a wind, spectral broadening occurs because the scattering angles and the distances from source to turbulent eddies and from the eddies to the detector are time-dependent. The analog in everyday experience is what you hear when an approaching car's horn is blowing at frequency ν_s and then recedes while you are standing to one side of the car's path: You actually hear the whole Doppler-shifted frequency range, from $\nu_s(1+\beta)$ to $\nu_s(1-\beta)$, as a function of time. (For scattered waves, the factors are $1 \pm 2\beta$, where $\beta =$ (speed of object/speed of sound), to first order in β.)

The second principle is that large objects (compared to the wavelength) scatter strongly but mainly in the near-forward direction, while small objects scatter weakly but nearly isotropically. Thus from large eddies, we get only a small spectral width, while from small eddies, we get $\pm 2\beta\nu_s$ but less amplitude.

Of course, in actuality the turbulent flow in a frame comoving with the mean wind is also time-dependent. But we have shown via these general principles and a computer model that this time dependence is unnecessary to explain the general features of some observed acoustic data. This is markedly in contrast to the conventional treatment of spectral broadening, which attributes all of spectral broadening to time dependence in the comoving frame. In that treatment, the source and detector are assumed to be in the far field of the whole turbulent scattering volume, so that, effectively, scattering angles and distances are not time-dependent. This is an unrealistic assumption for acoustics, where both the source and detector are invariably in the near field of the scattering volume.

One of the approximations apparently made in the theory developed in this report was the assumption of a "uniform" mean wind and a "uniform" ambient temperature. (The commonly used ambient temperature is taken as the mean temperature in the scattering volume V_s; we did not so restrict our ambient temperature.) But these may only be "apparent" approximations. For example, suppose we define the mean wind as the time and space averaged wind over the time of an experiment and over the whole scattering volume from the ground up. Then of course it is by definition uniform and constant, so "all" wind variations are part of the turbulent flow. This point of view would introduce anisotropy and/or inhomogeneity in the turbulent flow, which is easy to do in a turbule model. Also, suppose we define the mean temperature as the same time and space average of the nonacoustic temperature. Then all nonacoustic variations of temperature in V_s

are part of the turbulence. For example, suppose we used thermometers to "measure" a "mean temperature," and found these readings to be a function of height only, in V_s; typically, they would decrease with height. We could model this in terms of a constant ambient T_0, the average over height of the thermometer readings, plus turbules whose amplitudes ΔT did not cancel on average and depended on height in such a way as to reproduce the thermometric results. This method would introduce inhomogeneity in the turbulent temperature variations, and again this is easy to do with a turbule model. These ideas may be worth further investigation. However, this approach would not allow for the curved limiting ray paths that create shadow zones in the source radiation patterns. This curvature is small and was neglected in this work, because we treated scattered radiation only.

Another approximation that was made in the theory and thus in the developed code was that the source and detector are instantaneously in the radiation zone of any turbule, i.e., that R^{TS} and R^{DT} are large compared to the larger of $(\lambda, a^2/\lambda)$, at all times. This is not true at all times for all turbules in realistic scenarios, in which a few of the turbules may actually intercept the source and/or detector and in which a substantial fraction of the large turbules spend some time close to the source and detector. The radiation zone expressions were used as a compromise, because they yield the same results as the conventional theory in the limit of $\beta \to 0$. We expect that corrections to this approximation would not alter the general character of the total $|\tilde{A}(\omega)|$, but this expectation should be checked in the future. The fully correct theoretical expressions for the Born approximation scattered waves in near-field regions of a turbule can be obtained for the general model used, if we do not make the approximations mentioned just before equations (A-21), (A-37), and (A-52) and just after equations (A-38) and (A-39). But then, the expressions for the waves are extremely complicated and difficult to work with, so much so that it seems unlikely a three-dimensional model could be handled.

The computer code Slow Eddy developed in this work is not optimized. It can model a three-dimensional problem only roughly on a PC and only because the new time-shift algorithm is so much faster than direct computation. One improvement that might still be made in the code is to allow the scattering volume to be different for each turbule size: The larger the turbules, the smaller the volume needed. But a recipe for choosing the optimal scattering volumes is not so easy to attain, because the choices depend on virtually all the parameters of a scenario. It is probably best to experiment with this code to help determine how to modify it to use scale-dependent scattering volumes. Unfortunately, the effective volume needed increases inversely with turbule size, so this would not help much in reducing running time.

Other facets of an experimental scenario are that source waves reflected from the ground will be incident on the turbulence and that the source and/or the detector may be anisotropic. The latter could be modeled by suitable modifications of the computer code, along with some further

theoretical development. The former would require substantially more theoretical development and code alterations. The general character of scattered wave spectra may be altered appreciably by both effects.

Overall, the frequency spectra predicted by this model of time-dependent turbulence seem to have the same general characteristics as some observed spectra. How well this model applies to many different sets of experimental results needs to be tested. If it seems to work fairly well, then quite likely, it could be used to analyze acoustical remote sensing data with a view toward inferring detailed information about atmospheric turbulence and/or wind speeds.

References

1. G. H. Goedecke and H. J. Auvermann, "Acoustic scattering by atmospheric turbules," *J. Acoust. Soc. Am.* **102** (1997), pp 759–771.

2. V. I. Tatarskii, *The Effects of the Turbulent Atmosphere on Wave Propagation*, Keter, Jerusalem (1971).

3. A. S. Monin, "Characteristics of the scattering of sound in a turbulent atmosphere," *Sov. Phys. Acoust.* **7**, No. 130 (1962).

4. E. H. Brown and S. F. Clifford, "On the attenuation of sound by turbulence," *J. Acoust. Soc. Am.* **60** (1976), pp 788–793.

5. M. Galindo and D. I. Havelock, "Temporal coherence of a sound field in the turbulent atmosphere near the ground," *Proc. of the 7th International Symposium on Long-Range Sound Propagation*, Ecully, France (July 1966), pp 149–159.

6. H. J. Auvermann and G. H. Goedecke, "Influence of the Doppler effect on the bandwidth of acoustical signals scattered from atmospheric turbulence," *Proc. of the 8th International Symposium on Long-Range Sound Propagation*, Pennsylvania State University (9–11 September 1998).

Appendix A. Theoretical Derivations

A-1 Geometry and Model

See figure 1 of the main report. In the derivation that follows—

t	= clock time
x, y	= horizontal coordinates, $z =$ vertical coordinate
$\mathbf{r}$	= position vector
$\mathbf{w}$	= ambient wind velocity, uniform, constant
T_0	= ambient temperature
p_0	= ambient pressure
ρ_0	= ambient mass density
$\mathbf{R}^S$	$\equiv \mathbf{s}$ = source location
$\mathbf{R}^D$	$\equiv \mathbf{d}$ = detector location
$\mathbf{R}^T(t)$	$= \overline{\mathbf{R}}^T + \mathbf{w}t \equiv \bar{\mathbf{b}} + \mathbf{w}t$ = location of turbule "center"
$\mathbf{R}^{TS}$	$\equiv \mathbf{R}^T(t) - \mathbf{R}^S$
$\mathbf{R}^{DT}$	$\equiv \mathbf{R}^D - \mathbf{R}^T(t)$

The DS or ground-fixed frame is the "unbarred " frame (D, S = detector, source). The T (barred) frame is comoving with the wind (T = turbule). Their Cartesian coordinates are related by

$$\bar{x}_i = x_i - w_i t, \qquad \bar{t} = t \qquad \text{Galilean transformation.} \tag{A-1}$$

The total (temperature, pressure, mass density, and fluid velocity) fields in the DS system are

$$T(\mathbf{r},t) = T_0 + T_t(\mathbf{r},t) + T_a(\mathbf{r},t) \tag{A-2}$$
$$p(\mathbf{r},t) = p_0 + p_t(\mathbf{r},t) + p_a(\mathbf{r},t) \tag{A-3}$$
$$\rho(\mathbf{r},t) = \rho_0 + \rho_t(\mathbf{r},t) + \rho_a(\mathbf{r},t) \tag{A-4}$$
$$\mathbf{v}(\mathbf{r},t) = \mathbf{w} + \mathbf{v}_t(\mathbf{r},t) + \mathbf{v}_a(\mathbf{r},t)\,, \tag{A-5}$$

where the subscripts $(t, a) \equiv$ (turbulent, acoustic). In the T system, these fields are

$$\overline{T}(\bar{\mathbf{r}},\bar{t}) = T_0 + \overline{T}_t(\bar{\mathbf{r}},t) + \overline{T}_a(\bar{\mathbf{r}},t) \tag{A-6}$$
$$\bar{p}(\bar{\mathbf{r}},\bar{t}) = p_0 + \bar{p}_t(\bar{\mathbf{r}},t) + \bar{p}_a(\bar{\mathbf{r}},t) \tag{A-7}$$
$$\bar{\mathbf{v}}(\bar{\mathbf{r}},\bar{t}) = \bar{\mathbf{v}}_t(\bar{\mathbf{r}},t) + \bar{\mathbf{v}}_a(\bar{\mathbf{r}},t) \tag{A-8}$$
$$\bar{\rho}(\bar{\mathbf{r}},\bar{t}) = \rho_0 + \bar{\rho}_t(\bar{\mathbf{r}},t) + \bar{\rho}_a(\bar{\mathbf{r}}.t)\,, \tag{A-9}$$

where

$$\overline{T}(\bar{\mathbf{r}}.\bar{t}) = T_t(\mathbf{r}.t).\ldots.\bar{\mathbf{v}}_t(\bar{\mathbf{r}}.t) = \mathbf{v}_t(\mathbf{r}.t)|_{\mathbf{r}=\bar{\mathbf{r}}-\mathbf{w}t} \qquad \text{(A-10)}$$

and similarly for acoustic quantities.

We assume that the source emits uniformly in 4π and that the ground is totally absorbing; i.e., we ignore ground reflections.

A-2 Acoustic Equations

In the barred (comoving) frame, the relevant acoustic equations are the usual ones:

$$\partial_t \bar{v}_{ai} + \rho_0^{-1}\bar{\partial}_i \bar{p}_a = -\left(\overline{T}_T/\rho_0 T_0\right)\bar{\partial}_i \bar{p}_a - \bar{v}_{aj}\bar{\partial}_j \bar{v}_{Ti} - \bar{v}_{Tj}\bar{\partial}_j \bar{v}_{ai}\ . \qquad \text{(A-11)}$$

$$\partial_t \bar{p}_a + \gamma_h p_0 \bar{\partial}_i \bar{v}_{ai} = -\bar{v}_{Ti}\bar{\partial}_i \bar{p}_a + \overline{S}_a\ . \qquad \text{(A-12)}$$

The partial derivative symbols are $\partial_t = \partial/\partial t$ and $\partial_i = \partial/\partial x_i$ and $x_i = x.x_2 = y.$ and $x_3 = z$ in the stationary frame. The $\bar{\partial}_r$, etc, are partial derivatives in the comoving frame, where γ_h is the ratio of specific heat at constant pressure to the specific heat at constant volume.

In these equations, we have dropped terms in $\bar{p}_T$, since this is second order in $\bar{\mathbf{v}}_T$, and used the equation of state to put $\bar{p}_T/\rho_0 + \overline{T}_T/T_0 = \bar{p}_T/\rho_0 \approx 0$. Also, we have included a scalar acoustic source function $\overline{S}_a$ to be chosen. Note that the right-hand sides of these equations involve the turbulent temperature and velocity fluctuations $\overline{T}_T(\bar{\mathbf{r}}.t).\bar{v}_{Ti}(\bar{\mathbf{r}}.t)$; in this work, we regard them as stationary, i. e., $\overline{T}_T(\bar{\mathbf{r}}).\bar{v}_{Ti}(\bar{\mathbf{r}})$ only, with no explicit time dependence in the barred frame. They may be stochastic functions. Thus, in every detail, the description of the turbulence and acoustics in the barred frame is subjectively the same as in the standard description[1] in any reference frame with no wind.

The acoustic quantities in equation (A-11) and (A-12), the sum of the waves created by the source and the waves scattered by the turbulence, are written as

$$\bar{p}_a = \bar{p}_{ae} + \bar{p}_{as}\ . \qquad \bar{v}_{ai} = \bar{v}_{aei} + \bar{v}_{asi}\ .$$

in the Born approximation where the subscript e stands for "external," i.e., for the source waves that act as externally applied fields on the turbulence, and the subscript s stands for "scattered," representing waves scattered by the turbulence.

A-3 Source Wave

The "external" acoustic pressure and velocity waves in the barred (T) frame, generated by a scalar source, satisfy equations (A-11) and (A-12) with $\left(\bar{v}_{Ti}.\overline{T}_T\right) = 0$:

$$\partial_t \bar{p}_{ae} + \gamma_h p_0 \bar{\partial}_i \bar{v}_{aei} = \overline{S}_a(\bar{\mathbf{r}}.t) \qquad \text{(A-13a)}$$

[1] V. I. Tatarskii, *The Effects of the Turbulent Atmosphere on Wave Propagation*, Keter, Jerusalem (1971).

$$\partial_t \bar{v}_{aei} + \tfrac{1}{\rho_0}\bar{\partial}_i \bar{p}_{ae} = 0\ , \tag{A-13b}$$

where $\overline{S}_a(\bar{\mathbf{r}}.\,t)$ is the source term. From equation (A-13b), we may put

$$\bar{v}_{ae} = \bar{\partial}_i \bar{\Phi} \rightarrow \bar{p}_{ae} = -\rho_0 \partial_t \bar{\Phi}\ . \tag{A-14}$$

where $\bar{\Phi}$ is a "velocity potential." Then from equation (A-13a),

$$-\rho_0 \partial_t^2 \bar{\Phi} + \gamma_h p_0 \overline{\nabla}^2 \bar{\Phi} = \overline{S}_a\ .$$

Dividing by $\gamma_h p_0$ yields

$$(\overline{\nabla}^2 - \tfrac{1}{c^2}\partial_t^2)\bar{\Phi} = \tfrac{1}{\rho_0 c^2}\overline{S}_a\ , \qquad c^2 \equiv \gamma_h p_0/\rho_0\ , \tag{A-15}$$

where c is the adiabatic sound speed.

In the unbarred frame, the monochromatic isotropic point source is located at $\mathbf{r} = \mathbf{R}^S = \mathbf{s}$ and has frequency $\nu_s = \omega_s/2\pi$:

$$S_a(\mathbf{r}, t) = \mathcal{A}'\delta(\mathbf{r} - \mathbf{s})\exp(-i\omega_s t) + \text{c.c.}\ , \tag{A-16}$$

where $\mathcal{A}'$ is an amplitude and $\delta(\mathbf{r})$ is the Dirac delta. So, using equation (A-1),

$$\bar{S}_a(\bar{\mathbf{r}}, t) = \mathcal{A}'\delta(\bar{\mathbf{r}} - \mathbf{s} + \mathbf{w}t)\exp(-i\omega_s t) + \text{c.c.} \tag{A-17}$$

The Green function solution of equation (A-15) is

$$\bar{\Phi} = -\frac{\mathcal{A}'}{\rho_0 c^2}\frac{\exp(-i\omega_s t)}{4\pi}\int d^3\bar{r}'\frac{1}{\overline{R}}\delta(\bar{\mathbf{r}}' - \mathbf{s} + \mathbf{w}t - \boldsymbol{\beta}\overline{R})\exp(ik_s\bar{R}) + \text{c.c.}\ , \tag{A-18}$$

where $\boldsymbol{\beta} \equiv \mathbf{w}/c$, and

$$\overline{\mathbf{R}} \equiv \bar{\mathbf{r}} - \bar{\mathbf{r}}'. \tag{A-19}$$

We note that, with $\boldsymbol{\eta} \equiv \bar{\mathbf{r}}' - \mathbf{s} + \mathbf{w}t - \boldsymbol{\beta}\overline{R}$,

$$\begin{aligned} \frac{\partial}{\partial \bar{r}_i}\delta(\bar{\mathbf{r}}' - \mathbf{s} + \mathbf{w}t - \boldsymbol{\beta}\overline{R}) &= \frac{\partial\delta}{\partial\eta_j}\frac{\partial\eta_j}{\partial\bar{r}_i} = \left(\frac{\partial\delta}{\partial s_j}\beta_j\right)\widehat{\overline{R}}_i \\ \partial_t\delta(\bar{\mathbf{r}}' - \mathbf{s} + \mathbf{w}t - \boldsymbol{\beta}\overline{R}) &= \frac{\partial\delta}{\partial\eta_j}\frac{\partial\eta_j}{\partial t} = -c\left(\frac{\partial\delta}{\partial s_j}\beta_j\right)\ . \end{aligned} \tag{A-20}$$

Also, we neglect $\bar{\partial}_i\left(1/\overline{R}\right) = -\widehat{\overline{R}}_i/\overline{R}^2$ compared to $(1/\overline{R})\,ik_s\partial_i\overline{R}_i = ik_s\widehat{\overline{R}}_i/\overline{R}$, since we will have $k_s\overline{R} \gg 1$ always. So we have from equations (A-14), (A-18), and (A-20)

$$\bar{p}_{ae}(\bar{\mathbf{r}}, t) = \rho_0 c\left(ik_s + \boldsymbol{\beta}\cdot\nabla_s\right)\bar{\Phi} + \text{c.c.}\ , \tag{A-21}$$

$$\bar{\mathbf{v}}_{aei}(\bar{\mathbf{r}}, t) = \left(ik_s + \boldsymbol{\beta}\cdot\nabla_s\right)\overline{U}_i + \text{c.c.}\ , \tag{A-22}$$

where

$$\bar{\Phi} \equiv -\frac{\mathcal{A}'}{4\pi\rho_0 c^2}\int d^3\bar{r}'\frac{1}{\overline{R}}\delta(\bar{\mathbf{r}}' - \mathbf{s} + \mathbf{w}t - \boldsymbol{\beta}\overline{R})\exp(ik_s\bar{R})\exp(-i\omega_s t)\,. \tag{A-23}$$

$$\overline{U}_i \equiv -\frac{\mathcal{A}'}{4\pi\rho_0 c^2}\int d^3\bar{r}'\frac{\widehat{\overline{R}}_i}{\overline{R}}\delta(\bar{\mathbf{r}}' - \mathbf{s} + \mathbf{w}t - \boldsymbol{\beta}\overline{R})\exp(ik_s\bar{R})\exp(-i\omega_s t)\,. \tag{A-24}$$

The integrals in equations (A-23) and (A-24) can be done. Transform the variables by

$$\eta_i = \bar{\mathbf{r}}'_i - s_i + w_i t - \beta_i\overline{R}\,. \tag{A-25}$$

Then

$$\frac{\partial\eta_i}{\partial\bar{r}'} = \delta_{ij} + \beta_i\widehat{\overline{R}}_j\,. \qquad \text{since } \frac{\partial\overline{R}}{\partial\bar{r}'_j} = -\frac{\partial\overline{R}}{\partial\bar{r}_j} = -\widehat{\overline{R}}_j\,. \tag{A-26}$$

So the Jacobian is

$$J\left(\frac{\eta}{\bar{r}'}\right) = 1 + \boldsymbol{\beta}\cdot\widehat{\overline{\mathbf{R}}}\,. \tag{A-27}$$

Then the integrals involve $\delta(\eta)$, so we get

$$\bar{\Phi} = -\frac{\mathcal{A}'}{4\pi\rho_0 c^2}\frac{\exp(-i\omega_s t)}{\overline{R} + \boldsymbol{\beta}\cdot\overline{\mathbf{R}}}\exp(ik_s\overline{R}), \quad \overline{U}_i = \widehat{\overline{R}}_i\bar{\Phi}\,. \tag{A-28}$$

Here, from equation (A-25)

$$\overline{\mathbf{R}} = \bar{\mathbf{r}} - \bar{\mathbf{r}}' = \bar{\mathbf{r}} - [\boldsymbol{\eta} + \mathbf{s} - \mathbf{w}t + \boldsymbol{\beta}\overline{R}]_{\eta=0} \equiv \overline{\mathbf{R}}^s - \boldsymbol{\beta}\overline{R}\,, \tag{A-29}$$

where

$$\overline{\mathbf{R}}^s \equiv \bar{\mathbf{r}} - \mathbf{s} + \mathbf{w}t = \bar{\mathbf{r}} - \bar{\mathbf{s}}(t) \tag{A-30}$$

is the instantaneous vector from the source to the observation point $\bar{\mathbf{r}}$. Then taking $\overline{\mathbf{R}}\cdot\overline{\mathbf{R}}$ from equation (A-29) yields

$$\overline{R}^2 = \left(\overline{R}^s\right)^2 - 2\boldsymbol{\beta}\cdot\overline{\mathbf{R}}^s\overline{R} + \beta^2\overline{R}^2, \quad \text{or}$$

$$\left(1-\beta^2\right)\overline{R}^2 + 2\boldsymbol{\beta}\cdot\overline{\mathbf{R}}^s\overline{R} - \left(\overline{R}^s\right)^2 = 0\,.$$

The solution is

$$\overline{R} = \gamma^2\left\{-\boldsymbol{\beta}\cdot\overline{\mathbf{R}}^s + \sqrt{\left(1-\beta^2\right)\left(\overline{R}^s\right)^2 + \left(\boldsymbol{\beta}\cdot\overline{\mathbf{R}}^s\right)^2}\right\}\,. \tag{A-31}$$

where

$$\gamma^2 = \left(1-\beta^2\right)^{-1}\,. \quad \text{as in relativity.} \tag{A-32}$$

Then

$$\boldsymbol{\beta}\cdot\overline{\mathbf{R}} = \boldsymbol{\beta}\cdot\overline{\mathbf{R}}^s - \beta^2\overline{R}\,. \tag{A-33}$$

So

$$\overline{R} + \boldsymbol{\beta}\cdot\overline{\mathbf{R}} = \tfrac{\overline{R}}{\gamma^2} + \boldsymbol{\beta}\cdot\overline{\mathbf{R}}^s = \sqrt{\left(1-\beta^2\right)\left(\overline{R}^s\right)^2 + \left(\boldsymbol{\beta}\cdot\overline{\mathbf{R}}^s\right)^2} \equiv \overline{D}^s. \tag{A-34}$$

Thus from equation (A-28),

$$\bar{\Phi} = -\frac{\mathcal{A}'}{4\pi\rho_0 c^2}\frac{\exp(-i\omega_s t)\exp(ik_s\overline{R})}{\overline{D}^s}, \quad \overline{U}_i = -\frac{\mathcal{A}'}{4\pi\rho_0 c^2}\frac{\exp(-i\omega_s t)\exp(ik_s\overline{R})}{\overline{D}^s}\widehat{\overline{R}}_i\,. \tag{A-35}$$

Then from equation (A-21),

$$\bar{p}_{ae}(\bar{\mathbf{r}},t) = \rho_0 c\left(ik_s + \beta_j\tfrac{\partial}{\partial s_j}\right)\bar{\Phi}\,. \tag{A-36}$$

But again we neglect $(\partial/\partial s_j)(1/\overline{D}^s)$ compared to $(ik_s/\overline{D}^s)(\partial/\partial s_j)\overline{R}$. Now from equations (A-30) and (A-31),

$$\overline{R}_j\left[\frac{\partial\overline{R}_j}{\partial s_i} = -\delta_{ij} - \beta_j\frac{\partial\overline{R}}{\partial s_i}\right] = \overline{R}\frac{\partial\overline{R}}{\partial s_i} = -\overline{R}_i - \left(\boldsymbol{\beta}\cdot\overline{\mathbf{R}}\right)\frac{\partial\overline{R}}{\partial s_i}\,,$$

so

$$\frac{\partial\overline{R}}{\partial s_i} = \frac{-\overline{R}_i}{\overline{R}+\boldsymbol{\beta}\cdot\overline{\mathbf{R}}} = -\frac{\overline{R}_i}{\overline{D}^s}\,. \tag{A-37}$$

Thus from equations (A-35) and (A-36)

$$\bar{p}_{ae}(\bar{\mathbf{r}},t) = -\frac{\mathcal{A}'}{4\pi c}\frac{ik_s}{(\overline{D}^s)}\left(1 - \frac{\boldsymbol{\beta}\cdot\overline{\mathbf{R}}}{\overline{D}^s}\right)\exp(-i\omega_s t)\exp(ik_s\overline{R}) + \text{c.c.}\,,$$

but $1 - (\boldsymbol{\beta}\cdot\overline{\mathbf{R}}/\overline{D}^s) = \overline{R}/\gamma^2\overline{D}^s$, so finally

$$\bar{p}_{ae}(\bar{\mathbf{r}},t) = -\frac{\mathcal{A}'}{4\pi c}\frac{ik_s\overline{R}}{\gamma^2(\overline{D}^s)^2}\exp(-i\omega_s t)\exp(ik_s\overline{R}) + \text{c.c.} \tag{A-38}$$

Again we have neglected $(\partial/\partial s_i)(1/\overline{D}^s)$ compared to $(ik_s/\overline{D}^s)(\partial\overline{R}/\partial s_i)$, since $k_s\overline{R}$ and $k_s\overline{D}^s \gg 1$ always.

Then from equation (A-22), we get similarly

$$\bar{\mathbf{v}}_{aei}(\bar{\mathbf{r}},t) = -\frac{\mathcal{A}'}{4\pi\rho_0 c^2}\left[\frac{ik_s\overline{R}_i}{\gamma^2(\overline{D}^s)^2}\right]\exp(-i\omega_s t)\exp(ik_s\overline{R}) + \text{c.c.} \tag{A-39}$$

We will also need $(\partial/\partial\bar{r}_i)\bar{p}_{ae}(\bar{\mathbf{r}},\bar{t})$. Again for the far-field condition $k_s\overline{R} >>> 1$, we have to find $\partial\overline{R}/\partial\bar{r}_i$. But just as in equation (A-37) and above,

$$\frac{\partial\overline{R}}{\partial\bar{r}_i} = \frac{\overline{R}_i}{\overline{D}^s}\,. \tag{A-40}$$

Thus

$$\frac{\partial \bar{p}_{ac}}{\partial \bar{r}_i} = \frac{\mathcal{A}' k_s^2}{4\pi c \gamma^2} \frac{\overline{R}\overline{R}_i}{(\overline{D}^s)^3} \exp(-i\omega_s t) \exp(ik_s \overline{R}) + \text{c.c.} \tag{A-41}$$

As $\beta \to 0$, $\overline{D}^s \to \overline{R}^s$, $\overline{\mathbf{R}} \to \overline{\mathbf{R}}^s$, $\gamma \to 1$, and from equation (A-38), we get

$$\bar{p}_{ac}(\bar{\mathbf{r}}, t) = -\frac{\mathcal{A}'}{4\pi c} \frac{ik_s}{\overline{R}^s} \exp(-i\omega_s t) \exp(ik_s \overline{R}^s) \,. \tag{A-42}$$

Thus, we could put in general

$$\frac{-ik_s \mathcal{A}'}{4\pi c} \equiv \mathcal{P}_c a' \,. \tag{A-43}$$

where a' = length, and $\mathcal{P}_c$ is thus the pressure amplitude of the wave from the source at a distance $\overline{R}^s = a'$ from the source in a still atmosphere. This relation identifies the significance of the arbitrary amplitude $\mathcal{A}'$.

A-4 Scattered Waves

In Born approximation, the scattered waves satisfy equations (A-11) and (A-12) with $(\bar{p}_{as}, \bar{v}_{asi})$ on the left-hand sides, but with $(\bar{p}_{ac}, \bar{v}_{aci})$ on the right-hand sides. By combining these equations again to eliminate $\bar{\partial}_i \bar{v}_{asi}$ and applying the usual solenoidal condition $\bar{\partial}_i \bar{v}_{Ti} = 0$ on the turbulent velocity, we get the Monin wave equation

$$\left(\bar{\partial}_i \bar{\partial}_i - c^2 \partial_t^2\right) \bar{p}_{as} = -\overline{T}_0^{-1} \bar{\partial}_i \left(\overline{T}_T \bar{\partial}_i \bar{p}_{ac}\right) - 2\rho_0 \bar{\partial}_i \bar{\partial}_j \left(\bar{v}_{Tj} \bar{v}_{aci}\right) \,, \tag{A-44}$$

where two terms have canceled via equation (A-13a), because we assume that $\bar{S}_a \equiv 0$, where the turbulence is nonzero.

We write

$$\bar{p}_{as} = \bar{p}_{as}^T + \bar{p}_{as}^v \,. \tag{A-45}$$

where $\bar{p}_{as}^T$ is due to the turbulent temperature fluctuations $\overline{T}_T$, the first term on the right-hand side of equation (A-44), and $\bar{p}_{as}^v$ is due to the turbulent velocity fluctuations $\bar{v}_{Tj}$, the second term on the right-hand side. Then the Green's function solutions of equation (A-44) are

$$\bar{p}_{as}^T(\bar{\mathbf{r}}, t) = \frac{\partial}{\partial \bar{r}_i} \left(\frac{1}{4\pi T_0}\right) \int d^3\bar{r}' \frac{\overline{T}'(\bar{\mathbf{r}}')}{|\bar{\mathbf{r}} - \bar{\mathbf{r}}'|} \left[\frac{\partial \bar{p}_{ac}(\bar{\mathbf{r}}', t')}{\partial \bar{r}_i'}\right]_{t'=t-|\bar{\mathbf{r}}-\bar{\mathbf{r}}'|/c} \tag{A-46}$$

$$\bar{p}_{as}^v(\bar{\mathbf{r}}, t) = \frac{\partial^2}{\partial \bar{r}_i \partial \bar{r}_j} \frac{2\rho_0}{4\pi} \int d^3\bar{r}' \frac{\bar{v}_j^T(\bar{\mathbf{r}}')}{|\bar{\mathbf{r}} - \bar{\mathbf{r}}'|} \bar{v}_{aci}\left(\bar{\mathbf{r}}', t - |\bar{\mathbf{r}} - \bar{\mathbf{r}}'|/c\right) \,. \tag{A-47}$$

where $\bar{\mathbf{r}}$ is now the observation point. After doing the indicated derivatives, we will put $\bar{\mathbf{r}} = \mathbf{d} - \mathbf{w}t$, $\mathbf{d} = \mathbf{R}^D$, the detector location.

A-5 Temperature Scattering

From equation (A-41), we have

$$\left[\frac{\partial \bar{p}_{ae}(\bar{\mathbf{r}}', t')}{\partial \bar{r}'}\right]_{t'=t-|\bar{\mathbf{r}}-\bar{\mathbf{r}}'|/c} = \frac{\mathcal{A}' k_s^2}{4\pi c \gamma^2} \frac{\overline{R}\overline{R}_i}{(\overline{D}^s)^3} \exp(ik_s \overline{R}) \exp(-i\omega_s t) \exp(ik_s \overline{R}^d) + \text{c.c.}\,. \tag{A-48}$$

where

$$\overline{\mathbf{R}}^d = \bar{\mathbf{r}} - \bar{\mathbf{r}}' \tag{A-49}$$

$$\overline{R}_i = \overline{R}_i^s - \beta_i \overline{R}\,, \qquad \overline{R} = \gamma^2 \left\{-\boldsymbol{\beta} \cdot \overline{\mathbf{R}}^s + \overline{D}^s\right\} \tag{A-50}$$

$$\overline{D}^s = \overline{R}^s \sqrt{(1-\beta^2) + \left(\boldsymbol{\beta} \cdot \widehat{\overline{\mathbf{R}}}^s\right)^2}\,, \tag{A-51}$$

but now,

$$\overline{R}_i^s = \bar{r}_i' - s_i + w_i t - \beta_i \overline{R}^d\,. \tag{A-52}$$

In the expression for $\bar{p}_{as}^T$ of equation (A-46), when we take $\partial/\partial \bar{r}_i$, we again neglect $(\partial/\partial \bar{r}_i)(1/\overline{R}^d)$ compared to $(ik_s/\overline{R}^d)(\partial/\partial \bar{r}_i)\left(\bar{R} + \bar{R}^d\right)$, since we will have $k_s \bar{R}^d >>> 1$ also.

Similarly, we neglect $(\partial/\partial)[\bar{r}_i \left(\overline{R}\overline{R}_i\right)/(\overline{D}^s)^3]$ also. So we will need

$$\frac{\partial}{\partial \bar{r}_i} \exp\left[ik_s\left(\bar{R} + \bar{R}^d\right)\right] = ik_s \frac{\partial}{\partial \bar{r}_i}\left(\bar{R} + \bar{R}^d\right) \exp\left[ik_s\left(\bar{R} + \bar{R}^d\right)\right]\,. \tag{A-53}$$

But

$$\frac{\partial \bar{R}^d}{\partial \bar{r}_i} = \widehat{\overline{R}}_i^d\,, \qquad \frac{\partial \bar{R}}{\partial \bar{r}_i} = \frac{\partial \bar{R}}{\partial \bar{R}_j^s}\frac{\partial \bar{R}_j^s}{\partial \bar{r}_i} = -\beta_j \frac{\partial \bar{R}}{\partial \bar{R}_j^s} \widehat{\overline{R}}_i^d\,. \tag{A-54}$$

Using equations (A-50), (A-51), and (A-54), we get

$$\frac{\partial \bar{R}}{\partial \bar{R}_j^s} = \frac{1}{\overline{D}^s}\left\{\bar{\mathbf{R}}_j^s - \beta_j \bar{\mathbf{R}}\right\} = \frac{\bar{\mathbf{R}}_j}{\overline{D}^s}\,,$$

whereby

$$\frac{\partial}{\partial \bar{r}_i}(\bar{R} + \bar{R}^d) = \widehat{\overline{R}}_i^d \left(\overline{D}^s - \boldsymbol{\beta} \cdot \bar{\mathbf{R}}_j^s + \beta^2 \bar{R}\right) \frac{\widehat{\overline{R}}_0^d \bar{R}}{\overline{D}^s}\,. \tag{A-55}$$

Then

$$\frac{\partial}{\partial \bar{r}_i} \exp\left[ik_s\left(\bar{R} + \bar{R}^d\right)\right] = ik_s \left(\widehat{\overline{R}}_i^d \bar{R}/\overline{D}^s\right) \exp\left[ik_s\left(\bar{R} + \bar{R}^d\right)\right]\,. \tag{A-56}$$

So from equations (A-46), (A-56), (A-41), and (A-43), we get

$$\bar{p}_{as}^{T}(\bar{\mathbf{r}},\bar{t}) = -\frac{k_s}{4\pi T_0}\frac{\mathcal{P}_e a'}{\gamma^2}\int d^3\bar{r}'\frac{\overline{RR}_i}{(\overline{D}^s)^3}\frac{\widehat{\bar{R}}_i^d}{\bar{R}^d}\overline{T}^T(\bar{\mathbf{r}}')\exp[ik_s(\bar{R}+\bar{R}^d)]\exp(-i\omega_s t) + \text{c.c.} \tag{A-57}$$

Now, the turbule is localized at $\bar{\mathbf{r}}' = \bar{\mathbf{b}}$; that is,

$$\overline{T}^T(\bar{\mathbf{r}}') = \overline{T}(\bar{\mathbf{r}}' - \bar{\mathbf{b}}) = \overline{T}(\boldsymbol{\xi}) \ . \tag{A-58}$$

Define

$$\boldsymbol{\xi} = \bar{\mathbf{r}}' - \bar{\mathbf{b}} \ . \tag{A-59}$$

and change variables in the integrand. Discard the $\boldsymbol{\xi}$ terms in the $\bar{R}, \bar{R}_i$, etc, in the numerator and denominator of equation (A-57), because $\bar{R}^d \gg \xi, \bar{R} \gg \xi$. But we must keep terms of order ξ in the exponent. That is, we write

$$\exp\left[ik_s\left(\bar{R}+\bar{R}^d\right)\right] \approx \exp\left[ik_s\left(\bar{R}+\bar{R}^d\right)\right]_{\boldsymbol{\xi}=0}\exp(-i\mathbf{K}\cdot\boldsymbol{\xi}) \ , \tag{A-60}$$

and this defines the vector $\mathbf{K}$. Then we put

$$\bar{\mathbf{r}} = \mathbf{d} - \mathbf{w}t = \bar{\mathbf{d}}(t), \quad \bar{\mathbf{r}}' = \bar{\mathbf{b}} + \boldsymbol{\xi} \ . \tag{A-61}$$

Then

$$\bar{\mathbf{R}}^d = \mathbf{d} - \mathbf{b} - \mathbf{w}t - \boldsymbol{\xi} = \mathbf{R}^{DT} - \boldsymbol{\xi} \ , \tag{A-62}$$

$$\bar{R}^d = R^{DT} - \widehat{\mathbf{R}}^{DT}\cdot\boldsymbol{\xi} \ . \tag{A-63}$$

where

$$\mathbf{R}^{DT} \equiv \mathbf{d} - \mathbf{b} - \mathbf{w}t \ . \tag{A-64}$$

Now we need $\overline{R}$ as a Taylor series in $\boldsymbol{\xi}$. Define $\bar{R}_0$ by

$$\bar{R}(\boldsymbol{\xi}) = \bar{R}_0 + \boldsymbol{\xi}\cdot\boldsymbol{\nabla}_b\bar{R} \ .$$

Here, $\bar{R}_0$ is $(\overline{R})_{\boldsymbol{\xi}=0} = (\overline{R})_{\bar{\mathbf{r}}'=\bar{\mathbf{b}}}$, with $\overline{R}$ defined by equations (A-49) to (A-51). After some algebra, the previous equations yield

$$K_i = k_s\left\{\widehat{R}_i^{DT} - \frac{\partial\bar{R}_0}{\partial\bar{b}_i}\right\} \ . \tag{A-65}$$

where here

$$\frac{\partial\bar{R}_0}{\partial\bar{b}_i} = \frac{1}{\overline{D}^s}\left(\delta_{ij} + \widehat{R}_i^{DT}\beta_j\right)\bar{R}_{0j} \ . \tag{A-66}$$

with

$$\bar{R}_j^s = \bar{R}_j^{TS} - \beta_j R^{DT} , \tag{A-67}$$

$$\bar{R}_0 = \gamma^2 \left\{ -\boldsymbol{\beta} \cdot \bar{\mathbf{R}}^s + \overline{D}^s \right\} \tag{A-68}$$

$$\overline{D}^s = \left[\left(1 - \beta^2\right) \left(\bar{R}^s\right)^2 - \left(\boldsymbol{\beta} \cdot \bar{\mathbf{R}}^s\right) \right]^{\frac{1}{2}} , \tag{A-69}$$

$$\bar{R}_{0i} = \bar{R}_i^s - \beta_i \bar{R}_0 . \tag{A-70}$$

Then for $\bar{p}_{as}^T$ ($\bar{\mathbf{r}} = \mathbf{d} - \mathbf{w}t.\, t$) (at the detector), we get from equation (A-57)

$$\bar{p}_{as}^T(\text{detector}) = A^T(t) \exp(-i\omega_s t) + \text{c.c.} , \tag{A-71}$$

where $A^T(t)$ is a complex-valued time-dependent amplitude.

$$A^T(t) = -\frac{k_s^2}{4\pi T_0} \frac{\mathcal{P}_e a'}{\gamma^2} \frac{\bar{R}_0^2 \hat{\bar{\mathbf{R}}}_0 \cdot \hat{\mathbf{R}}^{DT}}{(\overline{D}^s)^3 R^{DT}} \exp[ik_s(R_0 + R^{DT})] \widetilde{\overline{T}}(\mathbf{K}) , \tag{A-72}$$

with $\mathbf{K}$ given by equation (A-65) and the other vectors by equations (A-66) to (A-70). Here, $\widetilde{\overline{T}}(\mathbf{K})$ is the Fourier transform of $\overline{T}(\boldsymbol{\xi})$, given by

$$\widetilde{\overline{T}}(\mathbf{K}) \equiv \int d^3\xi \exp(-i\mathbf{K} \cdot \boldsymbol{\xi}) \overline{T}(\boldsymbol{\xi}) . \tag{A-73}$$

This is accurate only if the source and detector are in the far-field region of the turbule at any given instant. That is, we must have $R^{TS} \gg \lambda_s$, $R^{TS} \gg a$, and $R^{TS} \gg a^2/\lambda_s$, where a is the scale length of the turbule, $\lambda_s = 2\pi/k_s$, and similarly for R^{DT}.

This is also valid to all orders of β; computationally, we should use it, although *probably* only first order in β is needed, since we expect $\beta \lesssim 0.05$ in most realistic situations, except in strong storms. Note that $\beta = 0.01$ yields $w = 3.4$ m/s ≈ 7.6 mi/hr, so $\beta \leq 0.05 \rightarrow w \leq 38$ mi/hr, reasonable. But terms of order β^2 in $\mathbf{K}$ and in $\exp[ik_s(\bar{R}_0 + R^{DT})]$ might shift the phases noticeably, since $k_s = \omega_s/c = (2\pi)(500)/340 = 9.24$ m^{-1}. It *would* be accurate enough to keep only first-order terms in β in the term $\bar{R}_0(\bar{\mathbf{R}}_0 \cdot \hat{\mathbf{R}}^{DT})/(\bar{D}^s)^3 R^{DT}$, but that would save very little time in numerical computation, so the higher order terms are kept.

For simplicity, we use a Gaussian turbule,

$$\overline{T}(\boldsymbol{\xi}) = (\Delta T) \exp(-\xi^2/a^2) . \tag{A-74}$$

The size or scale of this is a. Then the Fourier transform is

$$\widetilde{\overline{T}}(\mathbf{K}) = \pi^{3/2} a^3 (\Delta T) \exp(-K^2 a^2/4) . \tag{A-75}$$

Consider the result equation (A-72) in the $\beta \to 0$ limit. Then

$$A^T(t) = \underbrace{\left[\frac{\mathcal{P}_e a' \exp(ik_s R^{TS})}{R^{TS}}\right]}_{\text{effective incident plane wave amplitude}} \underbrace{\left[\frac{-k_s^2}{4\pi T_0}\hat{T}(\mathbf{K})\cos\theta\right]}_{f_T(\theta)\ \text{scattering amplitude}} \underbrace{\left[\frac{\exp(ik_s r)}{r}\right]}_{\text{spherical outgoing wave from scatterer}} . \qquad \text{(A-76)}$$

where we have defined $R^{DT} \equiv r$. $\hat{\mathbf{R}}^{DT} = \hat{\mathbf{r}}$. $\hat{\mathbf{R}}^{TS} = \hat{\mathbf{k}}_s$. and, for $\beta \to 0$.

$$\overline{R}_0 = \hat{\mathbf{k}} R^{TS}. \qquad \overline{D}^s = R^{TS}. \qquad \hat{\overline{\mathbf{R}}}_0 \cdot \hat{\mathbf{R}}^{DT} = \cos\theta .$$

with θ the scattering angle. This $\bar{A}^T(t)$ agrees with equation (2) found in an earlier paper by Goedecke and Auvermann;[2] it is the Monin result for acoustic scattering by stationary turbulent temperature inhomogeneities.

The ΔT is the temperature fluctuation amplitude. For isotropic homogeneous turbulence, it scales with a as $|\Delta T_a| = |\Delta T_1|\,(a/a_1)^{1/3}$, as discussed in the main text. If T_0 is the mean temperature $\overline{T}$, then half the ΔT_a must be taken negative and the other half positive, but with the same magnitude for each a.

A-6 Velocity Scattering

From equations (A-39), (A-52), and (A-47), we see that we need

$$\frac{\partial}{\partial \bar{r}_i \partial \bar{r}_j} \exp[ik_s(\bar{R} + \bar{R}_d)] .$$

Previously, we found in equation (A-56)

$$\frac{\partial}{\partial \bar{r}_i} \exp[ik_s(\bar{R} + \bar{R}_d)] = ik_s \left(\hat{\overline{R}}_i^d \bar{R}/\overline{D}^s\right) \exp[ik_s(\bar{R} + \bar{R}_d)] .$$

We obtain the derivative of this here by once again neglecting $\partial\bar{R}/\partial\bar{r}_j$ compared to $k_s\overline{R}\,\partial\overline{R}/\partial\bar{r}_j$, valid since $k_s\overline{R} >>> 1$. So we get

$$\frac{\partial^2}{\partial \bar{r}_i \partial \bar{r}_j} \exp[ik_s(\bar{R} + \bar{R}_d)] \approx -k_s^2 \hat{\overline{R}}_i^d \hat{\overline{R}}_j^d \frac{\overline{R}^2}{(\overline{D}^s)^2} \exp[ik_s(\bar{R} + \bar{R}_d)] . \qquad \text{(A-77)}$$

So from equations (A-47) and (A-39),

$$\bar{p}_{as}^r(\bar{\mathbf{r}}, \bar{t}) = -k_s^2 \frac{1}{2\pi c} \int d^3\bar{r} \left[\left((\mathcal{P}_e a') \frac{\bar{R}_i}{\bar{r}^2 (\bar{D}^s)^2}\right) \frac{\hat{\bar{R}}_i^d \hat{\bar{R}}_j^d (\bar{R}^2)}{(\bar{D}^s)^2 (\bar{R}^d)}\right] \qquad \text{(A-78)}$$
$$\times \bar{v}_{tj}(\bar{\mathbf{r}}') \exp[ik_s(\bar{R} + \bar{R}^d)] \exp(-i\omega_s t) + \text{c.c.}$$

[2] G. H. Goedecke and H. J. Auvermann, "Acoustic scattering by atmospheric turbules," *J. Acoust. Soc. Am.* **102** (1997), pp 759–771.

Now we put

$$\bar{v}_{tj}(\bar{\mathbf{r}}') \equiv \bar{v}_j\left(\bar{\mathbf{r}}' - \bar{\mathbf{b}}\right) \equiv \bar{v}_j\left(\boldsymbol{\xi}\right) \ . \tag{A-79}$$

and we put $\boldsymbol{\xi} = 0$ in the terms in the square bracket in the integrand. So there $\hat{\bar{R}}_i^d = \hat{\bar{R}}_i^{DT}$, $\overline{R}_i = \overline{R}_{0i}$, $\overline{R} = \overline{R}_0$, etc, as in equations (A-66) to (A-70), and also

$$\exp[ik_s(\bar{R} + \bar{R}^d)] = \exp[ik_s(\bar{R}_0 + R^{DT})]\exp(-i\mathbf{K}\cdot\boldsymbol{\xi}) \tag{A-80}$$

as in equation (A-60), where $\mathbf{K}$ is given by equation (A-65). Therefore, for $\bar{\mathbf{r}} = \bar{\mathbf{d}} - \mathbf{w}t$,

$$\begin{aligned} \vec{p}_{as}^{\,v}\ (\text{detector}) \ &= \left\{ -\frac{k_s^2 \mathcal{P}_e a'}{2\pi c}\frac{(\bar{R}_0)^3}{\gamma^2(\overline{D}^s)^4}\frac{\left(\hat{\bar{\mathbf{R}}}_0\cdot\hat{\mathbf{R}}^{DT}\right)\left(\hat{\mathbf{R}}^{DT}\cdot\tilde{\bar{\mathbf{v}}}(\mathbf{K})\right)}{R^{DT}} \right. \\ &\qquad \left. \times \exp[ik_s(\bar{R}_0 + R^{DT})] \right\} \exp(-i\omega_s t) + \text{c.c.} \\ &\equiv A^v(t)\exp[-i\omega_s t] + \text{c.c.}\ , \end{aligned} \tag{A-81}$$

where $A^v(t)$ is defined by the brace. Here,

$$\tilde{\bar{\mathbf{v}}}(\mathbf{K}) \equiv \int d^3\xi \exp(-i\mathbf{K}\cdot\boldsymbol{\xi})\bar{\mathbf{v}}\left(\boldsymbol{\xi}\right) \ . \tag{A-82}$$

For simplicity, we use a Gaussian turbule

$$\bar{\mathbf{v}}\left(\xi\right) = (\boldsymbol{\Omega}\times\boldsymbol{\xi})\exp(-\xi^2/a^2) \tag{A-83}$$

as in Goedecke and Auvermann's paper. Thus

$$\begin{aligned} \tilde{\bar{\mathbf{v}}}(\mathbf{K}) \ &= \ \boldsymbol{\Omega}\times i\nabla_K \int d^3\xi \exp(-i\mathbf{K}\cdot\boldsymbol{\xi})\exp(-\xi^2/a^2) \\ &= \ ia^3\pi^{3/2}\boldsymbol{\Omega}\times\nabla_K \exp(-K^2a^2/4) \quad \text{or} \\ \tilde{\bar{\mathbf{v}}}(\mathbf{K}) \ &= \ -\frac{ia^5\pi^{3/2}\Omega}{2}\left(\hat{\boldsymbol{\Omega}}\times\mathbf{K}\right)\exp(-K^2a^2/4)\ . \end{aligned} \tag{A-84}$$

For isotropic homogeneous turbulence, the energy transfer rate per unit mass, ε, from one turbule size to the next satisfies

$$\varepsilon \propto \left(v^2\right)(v/a) = \ (\text{independent of } a) \ \approx \Omega^3 a^2\ .$$

Thus $\Omega(a)$ scales with a as

$$\Omega(a) = \Omega(a_1)\left(\frac{a_1}{a}\right)^{2/3}, \qquad a_1 = a_{\max} = \ \text{largest turbule scale length used.} \tag{A-85}$$

So we put

$$\tilde{\bar{\mathbf{v}}}(\mathbf{K}) = -\frac{ia^5\pi^{3/2}}{2}\left(\Omega(a_1)a_1^{2/3}\right)a^{13/3}\left(\hat{\boldsymbol{\Omega}}\times\mathbf{K}\right)\exp(-K^2a^2/4)\,. \qquad \text{(A-86)}$$

In equation (A-84), $\hat{\boldsymbol{\Omega}}$ is a "randomly" oriented unit vector. If the turbulence is assumed to be isotropic, then $\hat{\boldsymbol{\Omega}}$ has a uniform probability distribution in 4π; that is, if we write

$$\hat{\boldsymbol{\Omega}} = \mathbf{e}_1\sin\theta_\Omega\cos\phi_\Omega + \mathbf{e}_2\sin\theta_\Omega\sin\phi_\Omega + \mathbf{e}_3\cos\theta_\Omega\,.$$

then

$$\begin{aligned} P_\theta(\theta_\Omega)\,d\theta_\Omega &= \frac{\sin\theta_\Omega d\theta_\Omega}{2} \rightarrow P_\theta(\theta_\Omega) = \frac{\sin\theta_\Omega}{2}\,. \\ P_\phi(\phi_\Omega)\,d\phi_\Omega &= \frac{d\phi_\Omega}{2\pi} \rightarrow P_\phi(\phi_\Omega) = \frac{1}{2\pi}\,. \end{aligned}$$

where $\left(P_\theta(\theta_\Omega)\,.\,P_\phi(\phi_\Omega)\right)$ are the probability distributions of $(\theta_\Omega\,.\,\phi_\Omega)$. If the turbulence is not taken to be isotropic, then a spherically symmetric rotating turbule model may not be adequate, and also $\hat{\boldsymbol{\Omega}}$ is not uniformly distributed in 4π.

Consider the result equation (A-81) in the limit $\beta = 0$. Insert $\bar{\mathbf{b}} = \mathbf{0} = \mathbf{b}$. Then $\hat{\mathbf{R}}^{TS} = \hat{\mathbf{k}}$; $\hat{\mathbf{R}}^{DT} = \hat{\mathbf{r}} = \hat{\mathbf{d}}$; $\bar{\mathbf{R}}_0 = \mathbf{R}^{TS}$; $\overline{D}^s = R^{TS}$; $R^{DT} = r$; so we get

$$\tilde{\bar{p}}^v_{as} = \underbrace{\left[\frac{\mathcal{P}_e a'\exp(ik_sR^{TS})}{R^{TS}}\right]}_{\substack{\text{effective incident}\\ \text{plane wave amplitude}}} \underbrace{\left[\frac{-k_s^2}{2\pi c}\cos\theta\left(\hat{\mathbf{r}}\cdot\tilde{\bar{\mathbf{v}}}(\mathbf{K})\right)\right]}_{\substack{f_v(\theta,\phi)\\ \text{scattering amplitude}}} \underbrace{\left[\frac{\exp(ik_sr)}{r}\right]}_{\substack{\text{spherical outgoing}\\ \text{wave from scatterer}}}\,. \qquad \text{(A-87)}$$

where here

$$\mathbf{K} = k_s\left(\hat{\mathbf{r}} - \hat{\mathbf{k}}\right)\,. \qquad \text{(A-88)}$$

Note that $\mathbf{K}\cdot\tilde{\bar{\mathbf{v}}}(\mathbf{K}) = 0$, since $\boldsymbol{\nabla}_\xi\cdot\bar{\mathbf{v}}(\boldsymbol{\xi}) = 0$, whereby $\hat{\mathbf{r}}\cdot\tilde{\bar{\mathbf{v}}}(\mathbf{K}) = \hat{\mathbf{k}}\cdot\tilde{\bar{\mathbf{v}}}(\mathbf{K})$ for $\beta = 0$. This scattering amplitude is the same as equation (2) of Goedecke and Auvermann's paper. (This is the Monin result for scattering by turbulent velocity fluctuations.)

We note that $\mathbf{K}\cdot\tilde{\bar{\mathbf{v}}}(\mathbf{K}) = 0$ in general, for any β, for the rotating sphere model (see eq (A-82)). In fact, this must be true for any turbulent eddy that satisfies $\boldsymbol{\nabla}_\xi\cdot\bar{\mathbf{v}}(\boldsymbol{\xi}) = 0$, because then

$$\int d^3\xi\exp(-i\mathbf{K}\cdot\xi)\boldsymbol{\nabla}_\xi\cdot\bar{\mathbf{v}}(\boldsymbol{\xi}) = 0 = i\mathbf{K}\cdot\tilde{\bar{\mathbf{v}}}(\mathbf{K})\,. \qquad \text{(A-89)}$$

where integration by parts and discard of the surface integral at "spatial infinity" yield the second equality. This surface integral must vanish since each turbule is localized. (We assume that turbules are "wholly contained" in the scattering volume.)

Appendix B. Computer Algorithm

B-1 Detector and Source Locations and Wind

The calculations are done in the "primed" coordinate system, which is ground-fixed but in which the wind is along the x' axis,

$$w_{x'} = w > 0, w_{y'} = w_{z'} = 0,$$

as in figure B-1. Define

$$x^{\mathrm{CM}} \equiv \frac{1}{2}(x^D + x^S).$$
$$y^{\mathrm{CM}} \equiv \frac{1}{2}(y^D + y^S).$$

The coordinate transformation is then

$$\begin{aligned} z' &= z, \\ x' &= (x - x^{\mathrm{CM}})\cos\alpha + (y - y^{\mathrm{CM}})\sin\alpha, \\ y' &= -(x - x^{\mathrm{CM}})\sin\alpha + (y - y^{\mathrm{CM}})\cos\alpha\ , \end{aligned} \tag{B-1}$$

and components of all position vectors are related in the same way. The user inputs the Cartesian components of $(\mathbf{R}^D, \mathbf{R}^S)$ and the magnitude w and azimuthal angle α of the horizontal wind velocity $\mathbf{w}$, in the "original" (unprimed) frame. The algorithm calculates the primed components of all vectors.

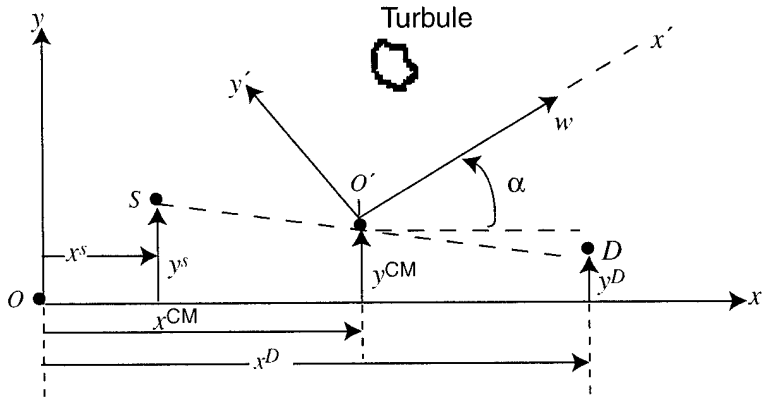

Figure B-1. "Primed" coordinate system.

B-2 Spectral Analysis

Consider the Fourier transform of equation (8) from the main report,

$$\tilde{p}_{as}^{T}(\omega) = \int_{-\infty}^{\infty} dt \exp(i\omega t) \left[A^{T}(t) \exp(-i\omega_s t) + A^{T*}(t) \exp(i\omega_s t) \right]$$

or

$$\tilde{p}_{as}^{T}(\omega) = \tilde{A}^{T}(\omega - \omega_s) + \tilde{A}^{T*}(\omega + \omega_s) \; . \tag{B-2}$$

Therefore, all we need to calculate is

$$\tilde{A}^{T}(\omega) \equiv \int_{-\infty}^{\infty} dt \exp(i\omega t) A^{T}(t) \tag{B-3}$$

and then use equation (B-2) if we wish. But the spectral broadening and shifting is all contained in $\tilde{A}^{T}(\omega)$, and similarly for the relation of $\tilde{p}_{as}^{T}(\omega)$ to $\tilde{A}^{T}(\omega)$.

Since we use fast Fourier transform algorithms, we must establish the minimum number of time-series points needed for adequate accuracy. First, equation (42) from the main report shows that the frequencies in $\tilde{A}^{T}(\omega)$ are given (approximately) by $\left[\nu_s \beta \cdot \left(\widehat{\mathbf{R}}^{DT}(t) - \widehat{\mathbf{R}}^{TS}(t) \right) \right]$. This varies from a minimum of $-2\beta\nu_s$ to a maximum of $2\beta\nu_s$; so from the Nyquist criterion, we need for $\tilde{A}^{T}(\omega)$

$$\nu_{\max} = \left((2\Delta t)^{-1} \right) > 2\beta\nu_s \rightarrow \Delta t < (4\beta\nu_s)^{-1} \; . \tag{B-4}$$

For example, for $\nu_s = 500$ Hz, $\beta = 0.01$, we need $\Delta t \lesssim 0.05$ s $\rightarrow \nu_{\max} \gtrsim 10$ Hz. The computer code uses an algorithm that yields these numbers for $\nu_s = 500$ Hz, $\beta = 0.01$. That is, it chooses

$$\nu_{\max} = \text{ integer value } \geq 2\beta\nu_s \; , \; \Delta t = (2\nu_{\max})^{-1} \; . \tag{B-5}$$

Second, we need appropriate frequency resolution. We can obtain an estimate of T_R (the minimum total time duration of a measurement that ensures adequate frequency resolution) by examining the scattered wave amplitude associated with large turbules with $k_s a \gg 1$. Consider figure B-2. For what values x_1 of x is the Gaussian reduced to perhaps e^{-4} of its maximum value? If $k_s a \gg 1$, x will be close to $D/2$. A little algebra yields

$$x_1 = \frac{D}{2} \pm \frac{1}{\sqrt{2} k_s a} \frac{(D^2 + 4h^2)^{3/2}}{Dh} \; . \tag{B-6}$$

Now use equation (42) from the main report to obtain ν_1 when $x = D/2$ and $x = x_1$. We easily get

$$\nu_1 \equiv \nu_{x=D/2} - \nu_{x=x_1} = \frac{\sqrt{2} w}{\pi a} \left(\frac{D^2 + 4h^2}{2Dh} \right) \; . \tag{B-7}$$

Figure B-2. Estimating minimum measurement time duration.

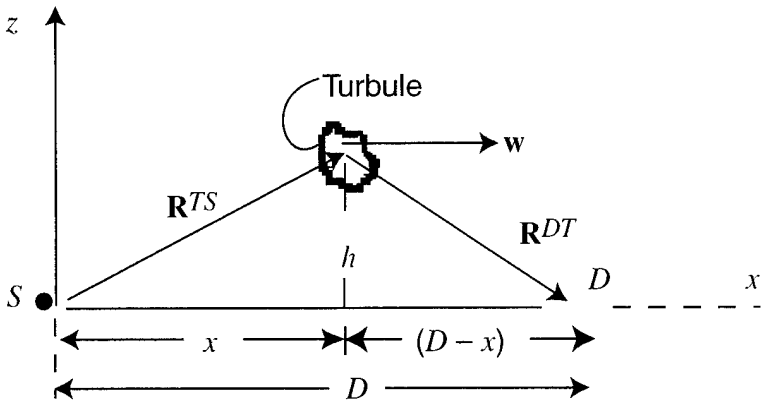

Essentially, only $-\nu_1 \lesssim \nu \lesssim \nu_1$ will be in the Fourier transforms of the amplitudes $A(t)$.

As w/a gets smaller, so does ν_1. The quantity $D^2 + 4h^2/2Dh$ has minimum value 2 for $h = D/2$. So

$$(\nu_1)_{\min} = \frac{\sqrt{2}w_{\min}}{\pi a_{\max}} . \tag{B-8}$$

Adequate frequency resolution requires perhaps $\Delta\nu \equiv T_R^{-1} \leq 10^{-1}\,(\nu_1)_{\min}$. We suppose that $a_{\max} = 10$ m, $w_{\min} = 1$ m/s. Then

$$T_R \gtrsim 10/\,(\nu_1)_{\min} = \frac{10\pi a_{\max}}{\sqrt{2}w_{\min}} \approx 200 \text{ s} . \tag{B-9}$$

Independently of this, we would like the total time T to be long enough to contain almost all the scattered pulse from one turbule that passes "symmetrically" over the source/detector. For small turbules, the scattered pulse amplitudes are approximately proportional to $\left(R^{DT}R^{TS}\right)^{-1}$. For source and detector positions both near the ground and a turbule passing directly overhead, as in figure B-3, the scattered amplitude is essentially a maximum when the turbule is at position 2, proportional to $R_{\min}^{-2}$, where

$$R_{\min} = \left((D/2)^2 + h^2\right)^{\frac{1}{2}} . \tag{B-10}$$

At positions 1 and 3, the amplitude is proportional to R^{-2}, where

$$R^2 \equiv \left((R_1 + D/2)^2 + h^2\right)^{\frac{1}{2}} \left((R_1 + D)^2 + h^2\right)^{\frac{1}{2}} . \tag{B-11}$$

For most scenarios, $h \ll D$ for turbules of interest, so we could neglect h in equations (B-10) and (B-11). Then we could require that we limit the length of the scattering volume along the wind direction (which is along $+x$ in this simple analysis) by requiring $R^2 \gtrsim 16R_{\min}^2$; this would include all signals within 6 percent of the maximum from a turbule that starts at $x = -R_1$ and travels the total distance $2R_1 + D$ in time T. For $h \approx 0$, this yields

$$(R_1 + D) \gtrsim 2D \rightarrow R_1 \gtrsim D . \tag{B-12}$$

Figure B-3. Estimating maximum measurement time duration.

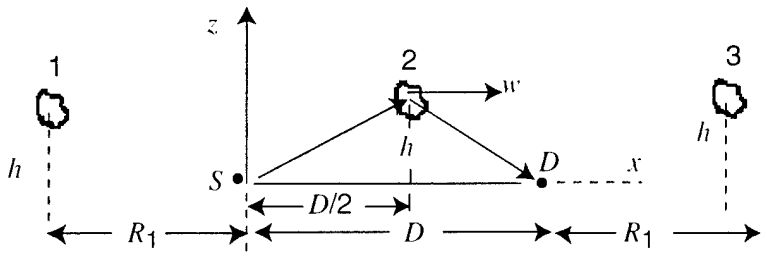

Then, the total length L of a tube along the wind would satisfy

$$L = D + 2R_1 \gtrsim 3D = 3|\mathbf{R}^{DS}| \,. \tag{B-13}$$

The computer algorithm uses the equality, and then chooses

$$T = L/w = 3|\mathbf{R}^{DS}|/w \,. \tag{B-14}$$

or uses $T = T_R$ given by equation (B-9), whichever is larger. For most cases of interest, equation (B-14) yields the larger value.

The minimum number of points N needed in the discrete time series for the $A(t)$ is then obtained by the use of equations (B-4) and (B-14),

$$N \gtrsim T/\Delta t = \frac{3R^{DS}4\beta\nu_s}{w} = \frac{6}{\pi}k_s R^{DS} \,. \tag{B-15}$$

or by the use of equations (B-4) and (B-9),

$$N \gtrsim T/\Delta t = \frac{10\pi a_{\max}2\beta\nu_s}{\sqrt{2}w} = \frac{10}{\sqrt{2}}k_s a_{\max} \,. \tag{B-16}$$

whichever is larger. Note that usually $R^{DS} \gg a_{\max}$.

Since N is used to dimension arrays, the FORTRAN source code actually defines a default value $N = 6048$ as a parameter. The user should verify that this is large enough to satisfy equations (B-15) and (B-16), and if it is not, change it and recompile. The values of T and L are calculated internally by putting $(T = (N-1)\Delta t.\ L = wT)$.

B-3 Turbule Model Parameters

As shown by Goedecke and Auvermann,[1] equations (67) and (68), for Kolmogorov spectra of isotropic homogeneous turbulence, the structure parameters (C_T^2, C_v^2) are related to the turbule parameters by

$$\begin{aligned} C_T^2 &= (3.78/\mu)(\phi)\left(\Delta T_1/a_1^{1/3}\right)^2 J_{8/3} \,, \\ C_v^2 &= (0.68/\mu)(\phi)\left(\Omega_1 a_1^{2/3}\right)^2 J_{14/3} \,. \end{aligned} \tag{B-17}$$

[1] G. H. Goedecke and H. J. Auvermann, "Acoustic scattering by atmospheric turbules," *J. Acoust. Soc. Am.* **102** (1997), pp 759–771.

where successively smaller turbule sizes a_α are related by

$$a_{\alpha+1}/a_\alpha = e^{-\mu} \equiv N_d^{-1} \,. \tag{B-18}$$

where $a_1 = a_{\max}$ is the outer scale length, $\phi = n_1 a_1 = n_\alpha a_\alpha$ is the packing fraction (the same for all sizes), and n_α is the number density of turbules of size α. $(\Delta T_1, \Omega_1)$ are the (temperature fluctuations, angular velocity) of the largest turbules, and here

$$J_s \equiv \int_0^\infty dx\, x^s e^{-x^2} = \frac{1}{2}\Gamma\left(\frac{s+1}{2}\right) \,. \tag{B-19}$$

where Γ is the gamma function. From tables of Γ functions,

$$\begin{aligned} J_{8/3} &= \frac{1}{2}\Gamma\left(\frac{11}{6}\right) \approx 0.47 \,. \\ J_{14/3} &= \frac{1}{2}\Gamma\left(\frac{17}{6}\right) = \frac{11}{12}\Gamma\left(\frac{11}{6}\right) \approx 0.86 \,. \end{aligned} \tag{B-20}$$

The $(\Delta T_\alpha, \Omega_\alpha)$ for size a_α are scaled from $(\Delta T_1, \Omega_1)$ as in equations (31) and (32) from the main report. The parameter $\mu = \ln N_d$ in equations (B-14) and (B-15) is calculated after the inner scale length a_{N_s}, the smallest turbule size, and the number of sizes N_s in the cascade are chosen by the user:

$$a_{N_s}/a_1 = \exp[-\mu(N_s - 1)] \rightarrow \mu = -(N_s - 1)^{-1} \ln(a_{N_s}/a_1) \,. \tag{B-21}$$

Default values are $N_s = 6$, $a_1 = 1.5$ m, $a_{N_s} = a_6 = 4.6875$ cm, which yield $\mu = \ln 2$, $N_d = 2$, i.e., a halving of sizes with each step. Doubling N_s while keeping (a_1, a_{N_s}) unchanged should approximately double the running time of the code. The effects of changing N_s, a_1, and/or a_{N_s} had not been investigated at the time of this writing.

Values of (C_T^2, C_v^2) may be input, in meter-kilogram-second units, and then the appropriate values of $(\Gamma_T = \Delta T_1/T_0,\ \Gamma_v = \Omega_1 a_1/c)$ are calculated. If the values $C_T^2 = C_v^2 = 0$ are input, then the code sets default values of $(\Delta T_1, \Omega_1)$ by putting

$$\Delta T_1/T_0 = \Gamma_T, \quad \Omega_1 a_1/c = \Gamma_v \,, \tag{B-22}$$

where (Γ_T, Γ_v) may be input. The algorithm begins calculating with the largest turbules (size a_1). It places the first tube of turbules of square cross section $d_1 = a_1/\phi^{1/3}$ along the wind direction (x'-axis) just on the y' side of the origin and centered along the x'-axis. The origin is chosen halfway between the source and the detector. That is, the centerline of the tube is $y' = d_1/2$, $z = R^S(3) + d_0 + d_1/2$. (The base of this tube is calculated to be d_0 m above the height of the source or detector above ground, whichever is greater.) The length of the tube is chosen by equation (B-13). Then at $t = 0$, one turbule is placed randomly inside each cubical cell of side length d_1 in the tube, such that each turbule center can have (x', y', z') displacements

from its cell center from 0 to $\pm d/4$ with equal independent probabilities. Then $(A^T(t), A^v(t))$ are calculated and accumulated for all these turbules. Any part of a turbule that leaves the tube (at $x' = L/2$) during time T is introduced at $x' = -L/2 + w\Delta t$, the next time step, thus keeping the frozen turbulence model in steady state.

Successive tubes for the largest turbules are chosen in such a way that tubes chosen later are further from the origin, in general. For example, the second tube would have a centerline $(y' = -d_1/2,\ z' = R^S(3) + d_0 + d_1/2)$. The third and fourth tubes would be above the first and second, respectively, with centerlines $(y' = \pm d_1/2,\ z' = R^S(3) + d_0 + 3d_1/2)$. The fifth and sixth tubes, if used, would be one step further away in y', with centerlines $y' = \pm 3d_1/2, z' = R^S(3) + d_0 + d_1/2$. This selection continues until input limits or default limits are reached.

For smaller turbules, successive tubes are chosen that fill all the largest tubes used. This implies, for example, that if $a_2 = a_1/2$, then there will be four times as many tubes of size $d_2 = a_2/\phi^{1/3} = d_1/2$ as there are for size d_1. It is impractical to calculate turbule by turbule for the smaller turbules, because there are so many of them. Instead, the time-shift algorithm is employed for turbules with $(R^{TS}, R^{DT}) \gtrsim (k_s d^2 \text{ or } k_s^{-1})$, whichever is larger, as described in the main report. The crucial values of R^{TS} and R^{DT} for this determination are the values for which the maximum signal occurs.

Appendix C. Quick Doppler Formula

Refer to figure 1 of the main report (p 3) for the geometry. The turbule is at $\mathbf{R}^T(t) = \mathbf{b}(t) = \mathbf{b}_0 + \mathbf{w}t$, where $\mathbf{w}$ = wind velocity. Pulses are emitted from the source S located at position $\mathbf{R}^S \equiv \mathbf{s}$ at times $t_1^S, t_2^S > t_1^S$ with $t_2^S - t_1^S \equiv \frac{2\pi}{\omega_s}$, ω_s = source angular frequency. Then the distances from the source to the turbule at times (t_1^T, t_2^T) are

$$\begin{aligned} R_1^{TS} &= |\mathbf{b}(t_1^T) - \mathbf{s}| = |\mathbf{b}_0 - \mathbf{s} + \mathbf{w}t_1^T| \,, \\ R_2^{TS} &= |\mathbf{b}_0 - \mathbf{s} + \mathbf{w}t_2^T| = |\mathbf{R}_1^{TS} + \mathbf{w}(t_2^T - t_1^T)| \\ &= R_1^{TS} + \mathbf{w} \cdot \widehat{\mathbf{R}}_1^{TS}(t_2^T - t_1^T) \,. \end{aligned} \tag{C-1}$$

Thus these pulses get to the turbule at times (t_1^T, t_2^T) given by

$$\begin{aligned} t_1^T &= t_1^S + \frac{R_1^{TS}}{c(1 + \boldsymbol{\beta} \cdot \widehat{\mathbf{R}}_1^{TS})} \approx t_1^S + \frac{R_1^{TS}}{c}(1 - \boldsymbol{\beta} \cdot \widehat{\mathbf{R}}_1^{TS}) \,, \\ t_2^T &= t_2^S + \frac{R_2^{TS}}{c(1 + \boldsymbol{\beta} \cdot \widehat{\mathbf{R}}_2^{TS})} \approx t_2^S + \frac{R_2^{TS}}{c}(1 - \boldsymbol{\beta} \cdot \widehat{\mathbf{R}}_2^{TS}) \\ &\approx t_2^S + \tfrac{1}{c}\left(R_1^{TS} + \mathbf{w} \cdot \widehat{\mathbf{R}}_1^{TS}(t_2^T - t_1^T)\right)(1 - \boldsymbol{\beta} \cdot \widehat{\mathbf{R}}_1^{TS}) \,, \end{aligned} \tag{C-2}$$

so

$$t_2^T - t_1^T = t_2^S - t_1^S + \boldsymbol{\beta} \cdot \widehat{\mathbf{R}}_1^{TS}(t_2^T - t_1^T) \approx (t_2^S - t_1^S)(1 + \boldsymbol{\beta} \cdot \widehat{\mathbf{R}}_1^{TS}) \,. \tag{C-3}$$

The distances from the turbule to a detector located at $\mathbf{R}^D = \mathbf{d}$ at times (t_1^T, t_2^T) are

$$\begin{aligned} R_1^{DT} &= |\mathbf{d} - \mathbf{b}_0 - \mathbf{w}t_1^T| \,, \\ R_2^{DT} &= |\mathbf{d} - \mathbf{b}_0 - \mathbf{w}t_1^T - \mathbf{w}(t_2^T - t_1^T)| \approx R_1^{DT}\left(\mathbf{w} \cdot \widehat{\mathbf{R}}_1^{DT}\right)(t_2^T - t_1^T) \,, \end{aligned} \tag{C-4}$$

so the times (t_1^D, t_2^D) at which the scattered pulses are received by the detector D are

$$\begin{aligned} t_1^D &\approx t_1^T + \frac{1}{c}R_1^{DT} \,, \\ t_2^D &\approx t_2^T + \tfrac{1}{c}R_2^{DT} \approx t_2^T + \frac{1}{c}R_1^{DT} - \left(\boldsymbol{\beta} \cdot \widehat{\mathbf{R}}_1^{DT}\right)(t_2^T - t_1^T) \,. \end{aligned} \tag{C-5}$$

Thus to order β,

$$t_2^D - t_1^D = \left(t_2^T - t_1^T\right)\left(1 - \boldsymbol{\beta}\cdot\widehat{\mathbf{R}}_1^{DT}\right) = (t_2^S - t_1^S)[1 - \boldsymbol{\beta}\cdot(\widehat{\mathbf{R}}_1^{DT} - \widehat{\mathbf{R}}_1^{TS})]\,. \tag{C-6}$$

Therefore the frequency observed at the detector is

$$\omega_{\rm obs} = \frac{2\pi}{t_2^D - t_1^D} \approx \omega_s(1 + \boldsymbol{\beta}\cdot(\widehat{\mathbf{R}}_1^{DT} - \widehat{\mathbf{R}}_1^{TS}))\,. \tag{C-7}$$

This is $\omega_{\rm obs}$ at D at time $t_1^D = t_1^T + \frac{1}{c}|\mathbf{d} - \mathbf{b}_0 - \mathbf{w}t_1^T| \approx t_1^S + \frac{1}{c}\left(R_1^{TS} + R_1^{DT}\right)$. Both $\widehat{\mathbf{R}}_1^{DT}$ and $\widehat{\mathbf{R}}_2^{TS}$ should be evaluated at time t_1^T in this formula for $\omega_{\rm obs}$. To first order in β, this is the same result obtained in the main report directly from the expressions for the waves $\left(p_{as}^T(t),\ p_{as}^v(t)\right)$ at the detector.

Appendix D. Computer Codes

This appendix contains descriptions of four FORTRAN codes. They are written in structured FORTRAN 77 standard form. The Microsoft International Mathematical and Statistical Library is used for random number generation and calculation of fast Fourier transforms. The Microsoft portlib routine TIMER() was used to time the codes. The codes are input.for used with sloweddy.for and input1.for used with slowone.for.

The input.for and input1.for codes write parameters to files. The parameters in the files can be edited by a text editor without having to rerun the input codes.

The description and code (with a list of symbols) for program input follow.

```
*************************************************************************
* Program Input                                                         *
* Version 1.0: 11-21-98                                                 *
*************************************************************************
* This program enters the environment parameters, and the turbule       *
* parameters needed for the Slow Eddy program. These parameters         *
* are written to the file "input.txt."                                  *
*************************************************************************
      PROGRAM INPUT
  IMPLICIT NONE
  INTEGER NMAX
  PARAMETER(NMAX=6400)

  CHARACTER CONFIG

  INTEGER IT,NS,NT

  REAL ALPHA,AP,A1,C,D(3),GAMT,GAMV,MW,NUS,PF
  REAL S(3),YC1(20),ZB,ZC1(20)

  OPEN(1,FILE='input.txt')

c  The following inputs have to do with the environment for the turbules.
  PRINT *
  PRINT *, 'Enter the sound speed in meters per second:'
  READ *, C

  PRINT *
  PRINT *, 'Enter the sound frequency of the source in Hertz:'
  READ *, NUS

  PRINT *
  PRINT *, 'Enter the reference distance'
  PRINT *, 'from the source in meters:'
  PRINT *, '(If not sure, enter 1)'
  READ *, AP

  PRINT *
  PRINT *, 'Enter the x,y,z coordinates'
  PRINT *, 'of the source in meters:'
  READ *, S

  PRINT *
  PRINT *, 'Enter the x,y,z coordinates'
  PRINT *, 'of the detector in meters:'
  READ *, D

  PRINT *
  PRINT *, 'Enter the boundary layer height in meters:'
  PRINT *, '(higher than either source or detector)'
  READ *, ZB

  IF((ZB.LE.S(3)).OR.(ZB.LE.D(3))) THEN
    PRINT *, 'The turbule(s) will pass through source or detector.'
    PRINT *, 'Please run the input program again, and enter a'
    PRINT *, 'boundary layer height greater than the source or'
    PRINT *, 'detector height.'
    STOP
  ENDIF
```

```
      PRINT *
      PRINT *, 'Enter the wind speed in meters per second:'
      READ *, MW

      PRINT *
      PRINT *, 'Enter the wind direction in degrees'
      PRINT *, 'measured counter clockwise from the x-axis:'
      READ *, ALPHA

C     The following inputs have to do with the turbules themselves.
      PRINT *
      PRINT *, 'Enter the size of the largest turbule in meters:'
      READ *, A1

      PRINT *
      PRINT *, 'Enter the packing fraction:'
      READ *, PF

      PRINT *
      PRINT *, 'Enter the temperature scale parameter:'
      READ *, GAMT

      PRINT *
      PRINT *, 'Enter the velocity scale parameter:'
      READ *, GAMV
      PRINT *
      PRINT *, 'Diagrams for configurations are given below:'
      PRINT *, '(hit "enter" to see more)'
      READ *
      PRINT *
      PRINT *, '    Configuration choices   '
      PRINT *
      PRINT *
      PRINT *, '             ----           '
      PRINT *, 'a:           |  |           '
      PRINT *, '             ----           '
      PRINT *
      PRINT *
      PRINT *, '          ----  ----        '
      PRINT *, 'b:        |  |  |  |        '
      PRINT *, '          ----  ----        '
      PRINT *
      PRINT *, '(hit "enter" to see more)'
      READ *
      PRINT *
      PRINT *, '          ----  ----        '
      PRINT *, '          |  |  |  |        '
      PRINT *, '          ----  ----        '
      PRINT *, '          ----  ----        '
      PRINT *, 'c:        |  |  |  |        '
      PRINT *, '          ----  ----        '
      PRINT *
      PRINT *
      PRINT *, '    ----  ----  ----  ----  '
      PRINT *, 'd: |  |  |  |  |  |  |  |  '
      PRINT *, '    ----  ----  ----  ----  '
      PRINT *
      PRINT *, '(hit "enter" to see more)'
```

```
      READ *
      PRINT *
      PRINT *, '           ----  ----         '
      PRINT *, '           |  |  |  |         '
      PRINT *, '           ----  ----         '
      PRINT *, '     ----  ----  ----  ----   '
      PRINT *, 'e:  |  |  |  |  |  |  |  |   '
      PRINT *, '     ----  ----  ----  ----   '
      PRINT *
      PRINT *
      PRINT *, '     ----  ----  ----  ----   '
      PRINT *, '     |  |  |  |  |  |  |  |   '
      PRINT *, '     ----  ----  ----  ----   '
      PRINT *, '     ----  ----  ----  ----   '
      PRINT *, 'f:  |  |  |  |  |  |  |  |   '
      PRINT *, '     ----  ----  ----  ----   '
      PRINT *
      PRINT *
      PRINT *, 'g:  User defined geometry:'
      PRINT *

      PRINT *
      PRINT *, 'Enter the letter (a-g) corresponding to the'
      PRINT *, 'the appropriate configuration desired.'
      PRINT *, '(make sure letter is lower case)'
      READ *, CONFIG
      PRINT *, 'Configuration chosen was ',CONFIG

      PRINT *
      PRINT *, 'Enter the total number of turbule sizes:'
      READ *, NS

c  If configuration g is chosen, the user will need to enter
c  the number a large tubes, and the y,z coordinates to the
c  center lines of these tubes.
            IF(CONFIG.EQ.'g') THEN
        PRINT *
        PRINT *, 'Enter the number of large tubes:'
        PRINT *, '(maximum number allowed is 20)'
        READ *, NT
              DO 5 IT=1,NT
          PRINT *
          PRINT *, 'Enter the Y and Z coordinates of the center'
          PRINT *, 'of large tube number',IT
          PRINT *, 'in dimensionless units:'
          READ *, YC1(IT),ZC1(IT)
5             CONTINUE
            ENDIF

c  All parameters entered above are written to the file 'input.txt'
c  used in the Slow Eddy FORTRAN program.
            WRITE(1,*) C
      WRITE(1,*) NUS
      WRITE(1,*) AP
      WRITE(1,*) S
            WRITE(1,*) D
      WRITE(1,*) ZB
            WRITE(1,*) MW
      WRITE(1,*) ALPHA
```

```
  WRITE(1,*) A1
  WRITE(1,*) PF
  WRITE(1,*) GAMT
  WRITE(1,*) GAMV
  WRITE(1,*) CONFIG
        WRITE(1,*) NS
    WRITE(1,*) NT
        DO 20 IT=1,20
          WRITE(1,*) YC1(IT),ZC1(IT)
20      CONTINUE

  CLOSE(1)

END
*-------------------------------------------------------------------------------*
*--------------------------------  List of Symbols  ----------------------------*
*-------------------------------------------------------------------------------*
*
* ALPHA    : real; angle of wind relative to non-rotated x-axis.
* AP       : real; 'a prime', reference distance from the source.
* A1       : real; size of largest turbule.
* C        : real; speed of sound.
* CONFIG   : character; abbreviation for 'configuration' used to choose
*            predefined tube configurations.
* D(3)     : real; position vector to the detector.
* GAMT     : real; 'capital gamma sub T'.
* GAMV     : real; 'capital gamma sub v'.
* IT       : integer; index for largest tube, with range from 1 to NT.
* MW       : real; 'magnitude of wind'.
* NMAX     : integer; maximum number of time (and frequency) data points
* NS       : integer; number of sizes of turbules.
* NT       : integer; number of largest tubes.
* NUS      : real; 'Greek letter nu sub s', the frequency
*            of the source.
* PF       : real; 'packing fraction'.
* S(3)     : real; position vector to the source.
* YC1(20)  : real; y coordinate to center line of largest tube, dimensionless.
* ZB       : real; height above ground where scattering volume begins.
* ZC1(20)  : real; z coordinate to center line of largest tube, dimensionless.

Descriptions of Program Slow Eddy and its eight subroutines and a list of symbols follows:

*********************************************************************************
* Program Slow Eddy *
* Version 1.0: 11-21-98                                  *
*********************************************************************************
* This program calculates the pressure amplitudes as a function of time,       *
* and their Fourier transforms as a function of frequency.  This program       *
* uses input from the file 'input.txt' that is generated by running the        *
* 'input.for' Fortran program.  The Slow Eddy program is designed to populate  *
* the scattering volume with tubes of turbules.  There are six predefined      *
* configurations (a-f) and one configuration choice specified by the user (g).*
* The tubes are populated with NS different sizes of turbules, keeping the     *
* packing fraction constant.  Each smaller size is obtained by halving the     *
* previous size. A separate program is provided to run one turbule by itself   *
* or one tube of turbules, all the same size. It is called 'slowone.for'.      *
* Subroutines: choise, direct, dot, multi, onetrb, output, rotate, tau.        *
*********************************************************************************
```

```
      PROGRAM MAIN

SUBROUTINE CHOICE(CONFIG)
c  This subroutine sets parameters for predefined configurations
c  chosen by the user in the 'input.txt' file.  It is assumed that
c  configuration a has been run before configuration b, etc.

SUBROUTINE DIRECT(AMPTT,AMPVT)
c  This subroutine calculates 'AMPTT' and 'AMPVT' one at a time and
c  accumulates the results directly (i.e., no time-shifting).
c  The 'MSIMSL' below stands for 'Microsoft International Mathematical
c  and Statistical Library'. MSIMSL contains a random number generator
c  that the 'DIRECT' subroutine uses.

SUBROUTINE DOT(V1,V2,V1V2)
c  This subroutine calculates the dot product of two, real, three
c  component vectors 'V1' and 'V2', and names this dot product 'V1V2'.

SUBROUTINE MULTI(AMPT,AMPV)
c  The 'MULTI' subroutine is a key subroutine in this program. It is named
c  'MULTI' because it is what drives the calculations for multiple tubes
c  with multiple turbules.

SUBROUTINE ONETRB(B0,AT,BV,K)
c  The 'ONETRB' subroutine calculates 'AT', BV', and 'K'
c  for one turbule, as the turbule travels the total length of
c  the tube. The 'ONETRB' subroutine is used by both the 'DIRECT'
c  subroutine, and the time-shifting 'TAU' subroutine.
c  The 'MSIMSL' subroutine library is need for the random number generator.

SUBROUTINE OUTPUT(AMPT,AMPV)
c  This subroutine takes the complex amplitudes 'AMPT' and 'AMPV'
c  as functions of time, and calculates the magnitude, and the real
c  and imaginary parts. It also performs the FFT on them.  Then the
c  subroutine writes the data to files called 'time.txt' and 'fft.txt'

SUBROUTINE ROTATE(ALPHA,MW)
c  The 'ROTATE' subroutine rotates the coordinate system so that the wind
c  direction is along the x-axis.  The origin is also moved to the point
c  located half way between the source and detector.

SUBROUTINE TAU(AMPTT,AMPVT)
c  The 'TAU' subroutine employs the time-shifting procedure.

*-----------------------------------------------------------------------*
*-------------------------------  List of Symbols  ---------------------*
*-----------------------------------------------------------------------*
* A           : real; characteristic size of turbule.
* AAT(NMAX)   : complex; temperature amplitude accumulation variable used
*               in the 'CHOICE' subroutine.
* AAV(NMAX)   : complex; velocity amplitude accumulation variable used
*               in the 'CHOICE' subroutine.
* AF          : real; 'angular frequency' equal to 2*Pi*nu_s.
* ALPHA       : real; angle of wind relative to non-rotated x-axis.
* AMPT(NMAX)  :  complex; amplitude due to temperature fluctuations.
* AMPTT(NMAX): complex; temperature amplitude accumulation variable for a
*               tube used in the 'DIRECT' and 'TAU' subroutines.
* AMPV(NMAX)  : complex; amplitude due to velocity fluctuations.
* AMPVT(NMAX): complex; velocity amplitude accumulation variable for a
```

```
*               tube used in the 'DIRECT' and 'TAU' subroutines.
* AT(NMAX)    : complex; temperature amplitude for one turbule used
*               in the 'ONETRB' subroutine.
* AT0(NMAX)   : complex; temperature amplitude for one turbule used
*               in the 'TAU' subroutine in the far field.
* AV(NMAX)    : complex; velocity amplitude for one turbule used
*               in the 'ONETRB' subroutine.
* AV0         : complex; velocity amplitude for one turbule used
*               in the 'TAU' subroutine in the far field.
* AP          : real; 'a prime', reference distance from the source.
* A1          : real; size of largest turbule.
* BCY         : real; y coordinate of centerline of largest tube.
* BCZ         : real; z coordinate of centerline of largest tube.
* BRK         : complex; 'bracket', a defined variable.
* BT          : real; the location of the turbule as a function of time.
* BTA(3)      : real; the Greek letter 'beta'. One of the
*               IMSL library subroutines used 'beta', so 'BTA' was used
*               as an alternate abbreviation.
* BTARS       : real; the dot product of 'BTA' and 'RS'.
* BTAR0       : real; the dot product of 'BTA' and 'R0'.
* BV(NMAX,3)  : complex; 'B sub v', a defined variable.
* B0(3)       : real; initial location of turbule.
* C           : real; speed of sound.
* CALPHA      : real; 'cosine of alpha'.
* COEF        : real; 'coefficient', a defined variable.
* CONFIG      : character; abbreviation for 'configuration' used to choose
*               predefined tube configurations.
* CPHI        : real; 'cosine of phi'.
* CROSS(3)    : real; the cross product of 'RDTH' and 'K'.
* CTEMP       : complex; a temporary complex variable.
* CTHETA      : real; 'cosine of theta'.
* D(3)        : real; position vector to the detector.
* DA          : real; distance between center of cells for size A.
* DCM(2)      : real; position vector to detector relative to 'center of mass'
*               position of source and detector.
* DI          : integer; time-shifting increment index.
* DNS         : real; distance between center of cells for smallest size.
* DS          : real; 'D sub s', a defined variable.
* DT          : real; time step increment.
* DTMAX       : real; maximum time step increment.
* DW(2)       : real; x and y components of position vector to detector
*               in the rotated 'wind' frame.
* D1          : real; distance between center of cells for largest size A1.
* ETA(3)      : real; Greek letter 'eta', random displacement vector.
* FAMPT(NMAX): complex; Fourier transform of 'AMPT'.
* FAMPV(NMAX): complex; Fourier transform of 'AMPV'.
* FRQ(NMAX)   : real; abbreviation for 'frequency', the independent variable
*               of the Fourier transform.
* GAMMA2      : real; abbreviation for 'lower case gamma, squared',
*               a defined variable.
* GAMT        : real; 'capital gamma sub T'.
* GAMV        : real; 'capital gamma sub v'.
* GAUSS       : real; 'gaussian', a variable that has a form that
*               resembles a gaussian function.
* I           : integer; time index, with range from 1 to N.
* IAMPT       : real; 'imaginary part of AMPT'.
* IAMPV       : real; 'imaginary part of AMPV'.
* II          : complex; the imaginary number 'i', the square root of -1.
* IM          : integer; index for turbule in a tube, with range from 1 to M.
```

```
* INS         : integer; number of time points in smallest cell.
* IS          : integer; index for sizes with range from 1 to NS.
* IT          : integer; index for largest tube, with range from 1 to NT.
* I1          : integer; number of time points in largest cell.
* J           : integer; index for vector components, with range 1 to 3.
* J2          : integer; running index for y component of a vector.
* J3          : integer; running index for z component of a vector.
* K(NMAX,3)   : real; a defined variable.
* KETA        : real; the dot product of 'K' and 'ETA'.
* KS          : real; wave number for the source 'k sub s'.
* L           : real; length of tubes.
* LMIN        : real; minimum length that tubes can have.
* M           : integer; number of turbules in a tube.
* MAMPT       : real; 'magnitude of AMPT'.
* MAMPV       : real; 'magnitude of AMPV'.
* MBTA        : real; 'magnitude of BTA'.
* MFAMPT      : real; 'magnitude of Fourier transform of AMPT'.
* MFAMPV      : real; 'magnitude of Fourier transform of AMPV'.
* MK          : real; 'magnitude of K'.
* MRDT        : real; 'magnitude of RDT'.
* MRS         : real; 'magnitude of RS'.
* MRTS        : real; 'magnitude of RTS'.
* MR0         : real; 'magnitude of R0'.
* MW          : real; 'magnitude of W'.
* M1          : integer; number of turbules in largest tube.
* N           : integer; number of time (and frequency) data points used.
* NMAX        : integer; maximum number of time (and frequency) data points
*               that can be used.
* NMIN        : integer; minimum number of time (and frequency) data points
*               that can be used.
* NS          : integer; number of sizes of turbules.
* NST         : integer; number of tubes in largest cell after each halving.
* NT          : integer; number of largest tubes.
* NUS         : real; 'Greek letter nu sub s', the frequency
*               of the source.
* OMEGAH(3)   : real; the unit vector 'omega hat'. Omega
*               is rotation velocity vector of a turbule.
* OMEGA1      : real; scaling parameter for the velocity turbules.
* PF          : real; 'packing fraction'.
* PHASE       : real; a defined variable in a complex exponent.
* PI          : real; variable for 3.14159...
* RAMPT       : real; 'real part of AMPT'.
* RAMPV       : real; 'real part of AMPV'.
* RDT(3)      : real; vector from turbule to detector.
* RDTH(3)     : real; 'RDT hat', unit vector in direction of 'RDT'.
* RN(4)       : real; a random number array.
* RNA(3)      : real; a random number array for angles.
* RNT(2)      : real; a random number array for temperature sign of + or -.
* RPHASE      : complex; abbreviation for the random phase, a defined variable.
* RS(3)       : real; a defined variable.
* RTS(3)      : real; vector from source to turbule.
* RTSH(3)     : real; abbreviation for 'RTS hat', a unit vector in the
*               direction of 'RTS'.
* R0(3)       : real; a defined variable.
* R0H(3)      : real; abbreviation for 'R0 hat', a unit vector in the
*               direction of 'R0'.
* R0RDTH      : real; the dot product of 'R0H' and 'RDTH'.
* S(3)        : real; position vector to the source.
* SALPHA      : real; 'sine of alpha'.
```

```
* SCM(2)      : real; position vector to source relative to 'center of mass'
*               position of source and detector.
* SIGMA2      : real; 'sigma squared', a defined variable.
* SPHI        : real; 'sine of phi'.
* STHETA      : real; 'sine of theta'.
* SW(2)       : real; x and y components of position vector to source
*               in the rotated 'wind' frame.
* T           : real; time variable.
* TEMP        : real; a temporary real variable.
* TIMER       : real; gives value of total time for the program to run.
* TMAX        : real; largest value of time variable.
* TS          : real; time for calculations for one size to be completed.
* TSF         : real; 'temperature scale factor', a defined variable.
* TWOPI       : real; '2*pi'.
* VSF         : real; 'velocity scale factor', a defined variable.
* V1(3)       : real; arbitrary vector used in the 'DOT' subroutine.
* V2(3)       : real; arbitrary vector used in the 'DOT' subroutine.
* V1V2        : real; result of the dot product of 'V1' and 'V2' in the
*               'DOT' subroutine
* W(3)        : real; wind velocity vector.
* XDS         : real; x component of the vector from the source
*               to the detector.
* YC          : real; y coordinate to center line of tube for size A.
* YC1(20)     : real; y coordinate to center line of tube for size A1.
* ZB          : real; height above ground where scattering volume begins.
* ZC          : real; z coordinate to center line of tube for size A.
* ZC1(20)     : real; z coordinate to center line of tube for size A1.
* ZI(3)       : real; Greek letter 'zi', random variable
*               between +1/4 and -1/4.
```

Descriptions of Program Input1 and Program Slow One follow:

```
*******************************************************************************
* Program Input1 *
* Version 1.0: 11-21-98 *
*******************************************************************************
* This program enters the environment parameters, and the turbule *
* parameters needed for the slowone.for program. These parameters *
* are written to the file "input1.txt." *
*******************************************************************************

*******************************************************************************
* Program Slow One *
* Version 1.0: 11-21-98                                    *
*******************************************************************************
* This program calculates the pressure amplitudes as a function of time,  *
* and their Fourier transforms as a function of frequency.  This program *
* uses input from the file 'input1.txt' that is generated by running the  *
* 'input1.for' Fortran program.  The Slow One program is designed to run *
* one tube of turbules of one size, or just one turbule by itself.   *
* Subroutines: choice, direct, dot, multi, onetrb, output, rotate, tau.      *
*******************************************************************************
```

Subroutines and symbols for Program Input1/Program Slow One are almost identical with those of Program Input/Program Slow Eddy.

Flow charts for Program Slow Eddy and its eight subroutines are given in figures D-1, D-2, D-3, D-4, and D-5.

Figure D-1. Flow chart for main program.

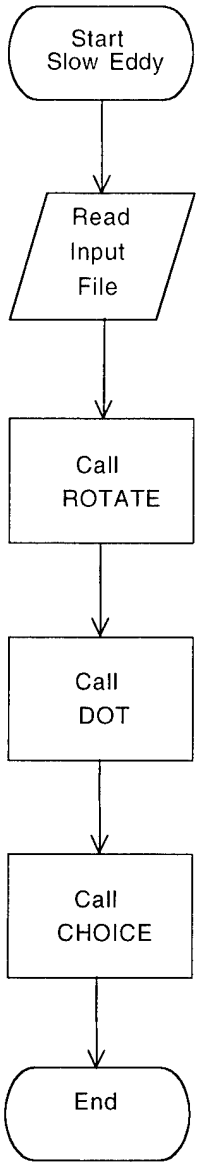

Figure D-2. Flow chart for subroutine CHOICE.

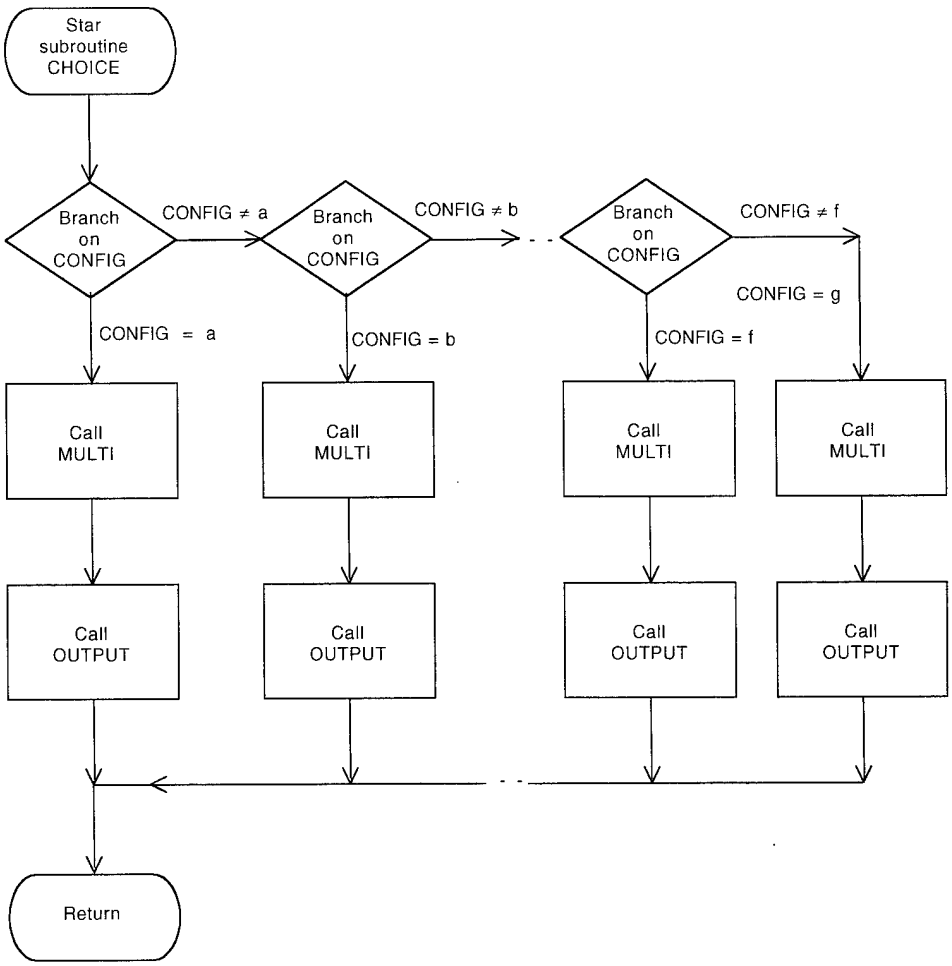

Figure D-3. Flow chart for subroutine MULTI.

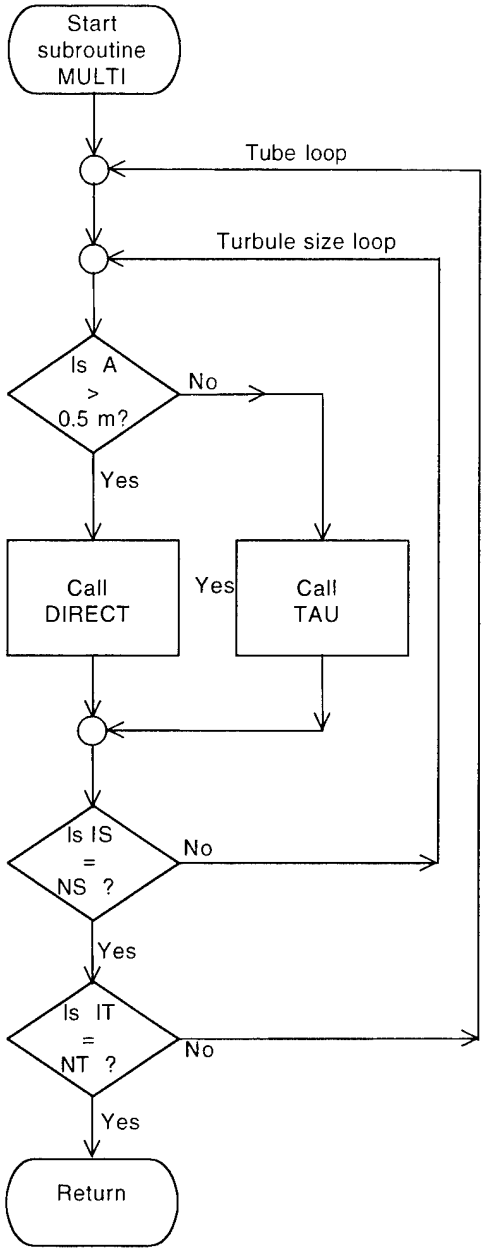

Figure D-4. Flow chart for subroutines ROTATE, DIRECT, and TAU.

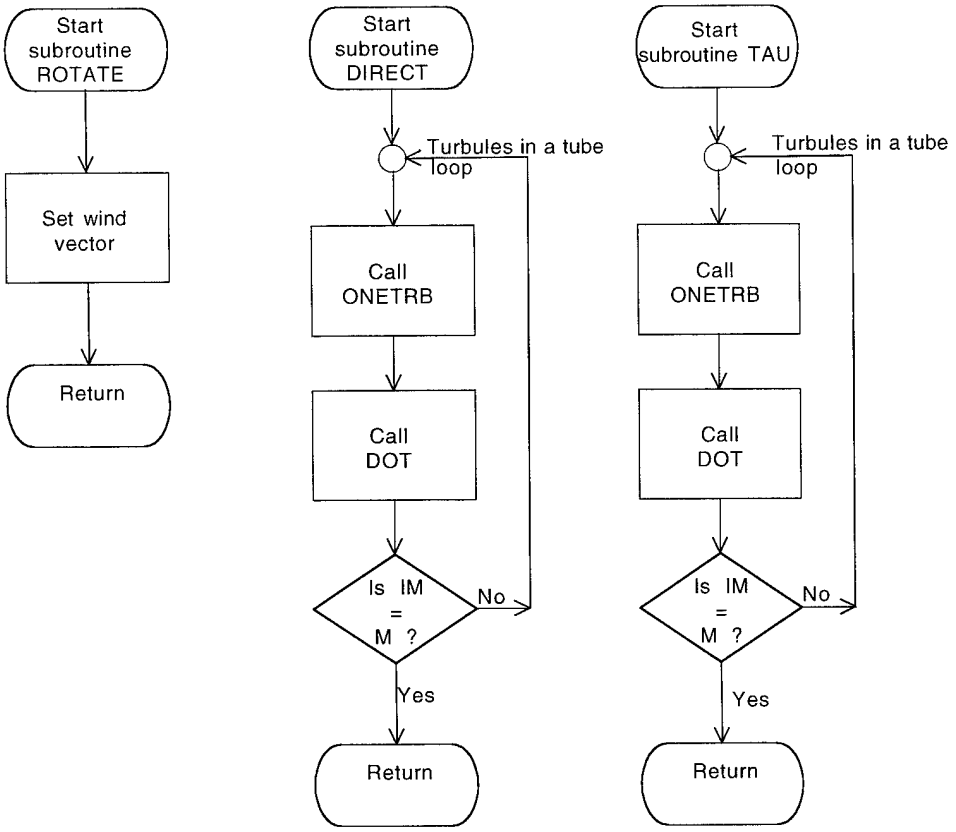

Figure D-5. Flow chart for subroutines ONETRB, OUTPUT, and DOT.

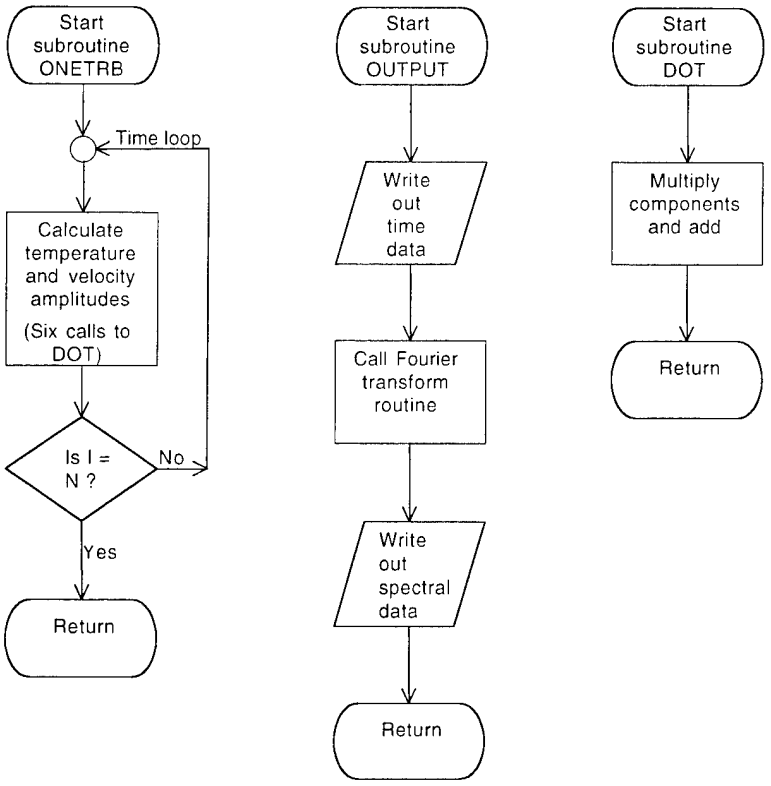

Not shown in figure D-2 for subroutine CHOICE is the intermediate save operations in branches for which the variable CONFIG is b through e. These are different in each branch, with typical file names given in table D-1.

Table D-1. Intermediate save operations.

CONFIG	File name(s)
b	cf12.txt
c	cf34.txt and cf1234.txt
d	cf56.txt
e	cf123456.txt*

*This branch does not call subroutine MULTI.

Distribution

Admnstr
Defns Techl Info Ctr
Attn DTIC-OCP
8725 John J Kingman Rd Ste 0944
FT Belvoir VA 22060-6218

Mil Asst for Env Sci Ofc of the Undersec of
Defns for Rsrch & Engrg R&AT E LS
Pentagon Rm 3D129
Washington DC 20301-3080

Ofc of the Secy of Defns
Attn ODDRE (R&AT)
The Pentagon
Washington DC 20301-7100

Ofc of the Secy of Defns
Attn OUSD(A&T)/ODDR&E(R) R J Trew
3080 Defense Pentagon
Washington DC 20301-7100

AMCOM MRDEC
Attn AMSMI-RD W C McCorkle
Redstone Arsenal AL 35898-5240

ARL Chemical Biology Nuc Effects Div
Attn AMSRL-SL-CO
Aberdeen Proving Ground MD 21005-5423

US Army Dugway Proving Ground
Attn STEDP 3
Attn STEDP-MT-DA-L-3
Attn STEDP-MT-M Bowers
Dugway UT 84022-5000

US Army Missile Cmnd
Attn AMSMI-RD-AS-SS R Alongi
Redstone Arsenal AL 35898-5253

US Army OEC
Attn CSTE EFS
4501 Ford Ave Park Center IV
Alexandria VA 22302-1458

Dir for MANPRINT
Ofc of the Deputy Chief of Staff for Prsnnl
Attn J Hiller
The Pentagon Rm 2C733
Washington DC 20301-0300

Hdqtrs Dept of the Army
Assist Secy of the Army for RD&A
Attn SARD-DOV H Fallin Rm 3E411
The Pentagon
Washington DC 20301-0103

Natl Security Agency
Attn W21 Longbothum
9800 Savage Rd
FT George G Meade MD 20755-6000

Redstone Scientific Info Ctr
Attn AMSMI-RD-CS-R
Bldg 4484
Redstone Arsenal AL 35898

SMC/CZA
2435 Vela Way Ste 1613
El Segundo CA 90245-5500

TECOM
Attn AMSTE-CL
Aberdeen Proving Ground MD 21005-5057

US Army ARDEC
Attn AMSTA-AR-TD M Fisette
Bldg 1
Picatinny Arsenal NJ 07806-5000

US Army CECOM RDEC
Night Vsn & Elect Sensors Dirctrt
Attn AMSEL-RD-NV-OD F Milton
10221 Burbeck Rd Ste 430
FT Belvoir VA 22060-5806

US Army CRREL
Attn CRREL-GP R Detsch
72 Lyme Rd
Hanover NH 03755-1290

US Army Info Sys Engrg Cmnd
Attn AMSEL-IE-TD F Jenia
FT Huachuca AZ 85613-5300

US Army Natick RDEC Acting Techl Dir
Attn SBCN-T P Brandler
Natick MA 01760-5002

Distribution (cont'd)

US Army Simulation, Train, & Instrmntn Cmnd
Attn AMSTI-CG M Macedonia
Attn J Stahl
12350 Research Parkway
Orlando FL 32826-3726

US Army Soldier & Biol Chem Cmnd Dir of Rsrch & Techlgy Dirctrt
Attn SMCCR-RS I G Resnick
Aberdeen Proving Ground MD 21010-5423

US Army Tank-Automtv Cmnd Rsrch, Dev, & Engrg Ctr
Attn AMSTA-TR J Chapin
Warren MI 48397-5000

US Army TRADOC Anlys Cmnd—WSMR
Attn ATRC-WSS-R
White Sands Missile Range NM 88002

US Army Train & Doctrine Cmnd
Battle Lab Integration & Techl Dirctrt
Attn ATCD-B
FT Monroe VA 23651-5850

US Military Academy
Mathematical Sci Ctr of Excellence
Attn MDN-A LTC M D Phillips
Dept of Mathematical Sci Thayer Hall
West Point NY 10996-1786

Nav Air War Cen Wpn Div
Attn CMD 420000D C0245 A Shlanta
1 Admin Cir
China Lake CA 93555-6001

Nav Surface Warfare Ctr
Attn Code B07 J Pennella
17320 Dahlgren Rd Bldg 1470 Rm 1101
Dahlgren VA 22448-5100

Naval Surface Weapons Ctr
Attn Code G63
Dahlgren VA 22448-5000

AF Rsrch Lab Phillips Lab Atmospheric Sci Div Geophysics Dirctrt
Hanscom AFB MA 01731-5000

Phillips Laboratory
Attn AFRL-VSBE Chisholm
29 Randolph Rd
Hanscom AFB MA 01731-3010

DARPA
Attn S Welby
3701 N Fairfax Dr
Arlington VA 22203-1714

NASA Marshal Spc Flt Ctr Atmos Sci Div
Attn Code ED 41 1
Huntsville AL 35812

Armstrong Atlantic State University
Attn R C Wood (2 copies)
11935 Abercorn Street
Savannah GA 31419-1997

New Mexico State Univ Dept of Physics
Attn G Goedecke (2 copies)
Las Cruces NM 88003-8001

Univ of Mississippi NCPA
Attn H E Bass
University MS 38577

Dept of Commerce Ctr
Mountain Administration
Attn Spprt Ctr Library R51
325 S Broadway
Boulder CO 80303

Hicks & Associates Inc
Attn G Singley III
1710 Goodrich Dr Ste 1300
McLean VA 22102

Natl Ctr for Atmospheric Research
Attn NCAR Library Serials
PO Box 3000
Boulder CO 80307-3000

NCSU
Attn J Davis
PO Box 8208
Raleigh NC 27650-8208

Distribution (cont'd)

Director
US Army Rsrch Ofc
Attn AMSRL-RO-D JCI Chang
Attn AMSRL-RO-EN W D Bach
PO Box 12211
Research Triangle Park NC 27709

US Army Rsrch Lab
Attn AMSRL-DD J M Miller
Attn AMSRL-CI-AI-R Mail & Records Mgmt
Attn AMSRL-CI-AP Techl Pub (3 copies)

US Army Rsrch Lab (cont'd)
Attn AMSRL-CI-LL Techl Lib (3 copies)
Attn AMSRL-IS-EE D K Wilson
Attn AMSRL-IS-EE H J Auvermann
(10 copies)
Attn AMSRL-SE-EE Z G Sztankay
Attn AMSRL-SE-SA N Srour
Adelphi MD 20783-1197

REPORT DOCUMENTATION PAGE

Form Approved
OMB No. 0704-0188

1. AGENCY USE ONLY *(Leave blank)*	2. REPORT DATE	3. REPORT TYPE AND DATES COVERED
	July 2000	Final, Oct 1997 to Aug 1999

4. TITLE AND SUBTITLE Doppler Broadening of Acoustic Waves Scattered by Turbulence Flowing With a Horizontal Wind

5. FUNDING NUMBERS
DA PR: B53A
PE: 61102A

6. AUTHOR(S) George H. Goedecke (New Mexico State University), Roy C. Wood (Armstrong Atlantic State University), Harry J. Auvermann (ARL)

7. PERFORMING ORGANIZATION NAME(S) AND ADDRESS(ES)
U.S. Army Research Laboratory
Attn: AMSRL-IS-EP email: hauverma@arl.mil
2800 Powder Mill Road
Adelphi, MD 20783-1197

8. PERFORMING ORGANIZATION REPORT NUMBER
ARL-TR-2131

9. SPONSORING/MONITORING AGENCY NAME(S) AND ADDRESS(ES)
U.S. Army Research Laboratory
2800 Powder Mill Road
Adelphi, MD 20783-1197

10. SPONSORING/MONITORING AGENCY REPORT NUMBER

11. SUPPLEMENTARY NOTES
ARL PR: 0FEJ60
AMS code: 61110253A11

12a. DISTRIBUTION/AVAILABILITY STATEMENT Approved for public release; distribution unlimited.

12b. DISTRIBUTION CODE

13. ABSTRACT *(Maximum 200 words)*

This report investigates the scattering of a monochromatic acoustic wave by an assumed unchanging atmospheric turbulence distribution that moves with a uniform constant horizontal wind. The source and detector are at rest at different positions in a ground-fixed frame. Theoretical expressions are derived for the scattered acoustic pressure at the detector. Because distances and scattering angles change with time as any turbulent fluctuation (turbule) flows through the scattering volume, the detector signal has a time-dependent Doppler frequency shift. A simple formula for the consequent frequency broadening is derived. A computer code is developed that calculates the scattered signal and its fast Fourier transform scattered by a single turbule, or by a collection of turbules of many different scale lengths. The code uses a new approximate but quite accurate time-shift algorithm that reduces the calculation time substantially. Several numerical results from this code are presented for a model scenario that is similar to a recent experimental scenario, with good agreement among spectral widths and shapes.

14. SUBJECT TERMS	15. NUMBER OF PAGES
Acoustic scattering, atmospheric turbulence, frequency spectrum	78
	16. PRICE CODE

17. SECURITY CLASSIFICATION OF REPORT	18. SECURITY CLASSIFICATION OF THIS PAGE	19. SECURITY CLASSIFICATION OF ABSTRACT	20. LIMITATION OF ABSTRACT
Unclassified	Unclassified	Unclassified	UL

NSN 7540-01-280-5500

Standard Form 298 (Rev. 2-89)
Prescribed by ANSI Std. Z39-18
298-102